Department of Physics and Astronomy
University of Heidelberg

Bachelor Thesis in Physics
submitted by

Christiane Katharina Maria Klein

born in Geldern (Germany)

2016

Study on neutrino beam experiments with multi-layer matter profiles

This Bachelor Thesis has been carried out by
Christiane Katharina Maria Klein
at the Max Planck Institut für Kernphysik in Heidelberg
under the supervision of
Prof. Manfred Lindner

Abstract

This thesis explores different unusual setups of neutrino oscillation experiments. They could help to observe parametric enhancement of neutrino oscillations or similar effects. Three different setups are studied: an artificial periodic step function density profile, a neutrino factory beam passing through the core of the earth, and a short baseline with two layers of matter of different constant densities. Different approximations of the neutrino oscillation probability and numerical calculations are used for analysing the setups giving an overview of the basic features. Only the neutrino beam through the earth is under certain conditions able to lead to observable enhancement effects coming from multiple layers of matter with different densities. However, the artificial density profile would have to be longer than 1000 km being technically not realizable. To detect parametric enhancement with a neutrino beam traversing the earth core, the energy resolution of the detector would have to be lowered to about 10%. In addition statistical analysis of the results to differentiate the used oscillation channels and high statistics are necessary. In the short baseline setup a vacuum layer of more than 300 km thickness would be needed to enhance matter effects. In experiments with atmospheric neutrinos the effects are small and washed out by experimantal energy resolution.

Abstract

In dieser Arbeit werden spezielle Aufbauten für Neutrinooszillationsexperimente untersucht. Sie sollen zur Beobachtung parametrischer Verstärkung von Neutrinooszillationen oder ähnlicher Effekte dienen. Es werden drei Aufbauten untersucht: ein künstliches Materieprofil mit einer periodischen Stufen-Dichtefunktion, ein Neutrinofabrikstrahl, der den Erdkern durchquert und eine kurze Baseline (Strecke zwischen Neutrinoquelle und Detektor) mit zwei Lagen Materie verschiedener Dichte. Zur Analyse dieser Aufbauten werden verschiedene Näherungen der Oszillationswahrscheinlichkeit und numerische Berechnungen genutzt, die einen Überblick über die grundlegenden Eigenschaften des jeweiligen Aufbaus geben. Es zeigt sich, dass sich nur beim Neutrinostrahl durch die Erde unter bestimmten Bedingungen verstärkende Materieeffekte beobachten lassen, die von Materie mit mehreren Lagen unterschiedlicher Dichte herrühren. Das künstliche Materieprofil müsste allerdings für solch eine Beobachtung mehr als 1 000 km lang sein, was technisch nicht realisierbar ist. Um parametrische Resonanz mit dem Neutrinostrahl durch die Erde detektieren zu können, müsste die Energieauflösung des Detektors auf 10 % gesenkt werden. Zudem wäre eine statistische Analyse zur Unterscheidung der verwendeten Oszillationskanäle und eine große Datenmenge nötig. Bei einer kurzen Baseline ist für verstärkende Effekte eine Strecke im Vakuum von mindestens 300 km nötig, was schwer zu realisieren ist. In Experimenten mit atmosphärischen Neutrinos ist der Effekt klein und wird zudem durch experimentelle Energieungenauigkeiten ausgewaschen.

Contents

1 Introduction

Since the discovery of neutrino oscillations [1], there have been various works on very different aspects of this phenomenon. Moreover, huge progress in determining the oscillation parameters has been made. Not long ago, a non-zero value for the oscillation parameter θ_{13} was found [2–4]. In addition to that, θ_{13} was found to be rather large, close to the upper bound from the Chooz reactor experiment [5]. Due to this, observations of the $\nu_e \to \nu_\mu$ oscillation channel mediated by θ_{13} are possible [1] .This provides opportunities for future experiments, since this is one of the main channels where matter effects can be observed.

For some neutrino sources, such as the sun, matter effects are quite sizeable. For other sources, especially artificial neutrino sources on earth, matter effects are often small. However, certain resonances cause big matter effects on neutrino oscillations, even for sources on the earth and rather short baselines in matter (compared to the way through the sun). There are two basic types of such resonances: The Mikheyev-Smirnov-Wolfenstein (MSW)-resonance [6, 7] and the parametric resonance [8, 9]. The MSW-resonance emerges from a certain relation between the neutrino energy and the matter density. The parametric resonance can occur for non-constant matter density profiles. It depends on the relation between the length scale of the matter density variations and the neutrino oscillations length in matter [10]. A realization that is easy to understand is a periodic matter density profile.

In this thesis, different realizations of neutrino beams traversing matter with a step function density profile will be discussed. Each of them will be studied to determine whether they can be employed to observe enhancement of neutrino oscillations which differs from the well established MSW-resonance phenomenon. This is interesting for two reasons. Firstly, there has been no experimental evidence for the parametric enhancement of neutrino oscillations so far. The situations

[1] This oscillation channel can also be mediated by the solar parameters θ_{12} and Δm^2_{21}. The dominant mediation depends on the baseline and neutrino energy.

discussed in this thesis might help to find a way to change that fact. Furthermore, the presented analysis can help to decide which setup is the most promising for the detection of one of those enhancing effects.

Secondly, the enhancement of matter effects of neutrino oscillations can help to measure another important parameter: the neutrino mass hierarchy. There have been measurements on the absolute mass squared difference between the two mass eigenstates which are closer in energy. They show that the mass of the mass eigenstate with larger ν_e-contribution, called ν_1, is smaller than the mass of the eigenstate with smaller ν_e-contribution, called ν_2. Thus, in this convention of naming the mass eigenstates, $\Delta m^2_{21} = m^2_2 - m^2_1 > 0$ holds (see, e.g. [11] for a recent review). Hence, two possibilities for the mass ordering remain. These are the normal ordering, also called normal hierarchy (NH), $m_1 < m_2 < m_3$, and the inverted ordering, also called inverted hierarchy (IH), $m_3 < m_1 < m_2$. The term mass hierarchy is sometimes used instead of the more general expression of mass ordering.

Frequently, the difference between the orderings appears as a difference in matter effects on neutrino oscillations. Therefore, enhancement of matter effects might play a role in the quest for the determination of the neutrino mass hierarchy. If the setups discussed here can disclose enhancement of matter effects, they might also be sensitive to the neutrino mass ordering. The motivation for the study of the three setups in this thesis is the observation of yet unobserved enhancement of matter effects on neutrino oscillations and the possibility to use this enhancement for the observation of the mass hierarchy.

The thesis is structured as follows: The chapters 1-3, are an introduction to the topic of neutrino oscillations. They provide the theoretical basics. Neutrino oscillations in vacuum and the evolution matrix formalism are introduced in chapter 2. In chapter 3 general matter effects on neutrino oscillations are described, and the oscillations probabilities in matter in the two-flavour approximation and for constant matter density are presented. In addition the parametric resonance of

neutrino oscillations is discussed.

This introduction is followed by the studies of three different setups for neutrino beam experiments. In chapter 4 the properties of neutrino oscillations in an artificial periodic density profile are described. Comments on the applicability of such a setup are given. Chapter 5 addresses the parametric resonance of neutrinos passing through the core of the earth. Chapter 6 is about the enhancement of matter effects for neutrino oscillations with short-baseline two-layer structures of the matter density profile.

Conclusions are drawn in chapter 7.

The calculations in this thesis are done in the natural units

$$\hbar = c = 1\,.$$

2 Neutrino oscillations in vacuum

In the first section of this chapter neutrino oscillations in vacuum in the two-flavour approximation are described. Neutrino oscillations have first been suggested by Pontecorvo [12, 13] and Maki, Nakagawa and Sakata [14]. The calculations in this section mostly follow the description in [15–17]. In a second section the evolution matrix approach is introduced.

At first, a neutrino produced in a charged-current weak interaction process is considered. The neutrino initially has the flavour a where a denotes one of the flavour eigenstates e, μ and τ. The reason is that flavour states are the eigenstates of weak interaction. The time development of this state, $\nu(t)$, in the flavour space can be described by a Schrödinger equation (see, e.g., [16])

$$i\frac{d}{dt}\left|\nu(t)\right\rangle = \mathcal{H}\left|\nu(t)\right\rangle\,, \tag{2.1}$$

where $\mathcal{H}$ is the Hamiltonian of the system. The Hamiltonian of a free, relativistic particle of mass m is given by the energy,

$$E = \sqrt{p^2 + m^2}\,. \tag{2.2}$$

However, the flavour states differ from the mass eigenstates which are the eigenstates of the free propagation. The mass and the flavour eigenstates are connected by the leptonic mixing matrix U:

$$|\nu_a\rangle = \sum_{i=1}^{3} U_{ai}^{*}\,|\nu_i\rangle\ . \tag{2.3}$$

The index i denotes the mass eigenstates 1,2 and 3. The mixing matrix U is also referred to as the Pontecorvo-Maki-Nakagawa-Sakata (PMNS) matrix [12–14]. Combining eq. (2.2) and eq. (2.3), equation (2.1) can be written as

$$i\frac{d}{dt}\,|\nu(t)\rangle = U diag(E_1, E_2, E_3)U^{\dagger}\,|\nu(t)\rangle\ . \tag{2.4}$$

This means the neutrino state at the time t can be described as

$$|\nu(t)\rangle = \sum_{j=1}^{3} U_{aj}^{*}\,|\nu_j\rangle\, e^{-iE_j t}\,, \tag{2.5}$$

where $|\nu_j\rangle$ is the state vector of the jth mass eigenstate (see, e.g. [17]) [2].

Finally, the probability for the neutrino to oscillate into the flavour state b is given by

$$P_{\nu_a\to\nu_b}(t) = |\langle\nu_b\,|\,\nu(t)\rangle|^2 \tag{2.6}$$

$$= |\sum_{j} U_{bj} e^{-iE_j t} U_{aj}^{*}|^2\,. \tag{2.7}$$

[2] To simplify the computation, it is assumed here that the different mass eigenstates have equal momenta. This is not entirely correct, but it reproduces the results of the consistent treatment with high accuracy. For a consistent treatment, the quantum mechanical wave packet approach or an approach based on quantum field theory should be used. See, e.g. [18, 19] for detailed explanation in the wave packet approach.

2.1 The two-flavour approximation

The existing data on neutrino oscillations is usually described in the context of three flavours. There are also contradictory indications of the existence of a fourth neutrino species. In this thesis, only the standard three-flavour approach is considered. In this context, the mixing matrix U is given as a combination of three rotations and one complex phase. Furthermore, the standard parametrization will be used. It is given by $U = R_{23}V_{13}R_{12}$. Here the matrices

$$R_{12} = \begin{pmatrix} c_{12} & s_{12} & 0 \\ -s_{12} & c_{12} & 0 \\ 0 & 0 & 1 \end{pmatrix} \text{ and } R_{23} = \begin{pmatrix} 1 & 0 & 0 \\ 0 & c_{23} & s_{23} \\ 0 & -s_{23} & c_{23} \end{pmatrix} \tag{2.8}$$

are rotation matrices in the 12- or 23- planes in flavour space and

$$V_{13} = \begin{pmatrix} c_{13} & 0 & s_{13}e^{-i\delta_{cp}} \\ 0 & 1 & 0 \\ -s_{13}e^{-i\delta_{cp}} & 0 & c_{13} \end{pmatrix} \tag{2.9}$$

is the rotation matrix in the 13-plane with an additional CP-phase[3]. The notation $s_{ij} = \sin\theta_{ij}, c_{ij} = \cos\theta_{ij}$ is applied where θ_{ij} is the corresponding mixing angle.

In this thesis, a two-flavour-approximation will often be utilized for various reasons. It simplifies calculations significantly, and even more important, it is quite accurate in many cases. The reason is that there are two small parameters characterizing neutrino oscillations, θ_{13} and $\frac{\Delta m^2_{21}}{\Delta m^2_{31}}$ (see, e.g., [22]). This leads to a nearly decoupling of different oscillation channels. The calculations in this chapter can, for example, be found in [23].

In the two flavour case, there is only one mixing angle, θ_0. In addition, the CP-violating phase drops out because it can be absorbed

[3]In [20] the author states that this parametrization is similar to the parametrization of the Cabibbo-Kobayashi-Maskawa-matrix (CKM-matrix) [21] in the quark sector.

by rephasing the neutrino fields. This means that U can be written as

$$U = \begin{pmatrix} c_0 & s_0 \\ -s_0 & c_0 \end{pmatrix} . \tag{2.10}$$

In the following, the notation $s_0 = \sin\theta_0$ and $c_0 = \sin\theta_0$ is applied. The two flavours will be e and x, where x can be either μ or τ or a combination thereof. Inserting this matrix into eq. (2.7), it is straightforward to calculate the oscillation probability $\nu_e \to \nu_x$:

$$\begin{aligned} P_{\nu_e \to \nu_x}(t) &= |\, \langle \nu_x \,|\, \nu_e(t) \rangle \,|^2 \\ &= |\, (-s_0 \langle \nu_1| + c_0 \langle \nu_2|) \left(c_0 |\nu_1\rangle e^{-iE_1 t} + s_0 |\nu_2\rangle e^{-iE_2 t} \right) |^2 \\ &= |s_0 c_0 \left(e^{-iE_2 t} - e^{-iE_1 t} \right) |^2 \end{aligned} \tag{2.11}$$

It is convenient to define

$$\delta_{ij} = \frac{E_i - E_j}{2} . \tag{2.12}$$

The energies of the mass eigenstates can be approximated by

$$E_i \simeq p + \frac{m_i^2}{2p} . \tag{2.13}$$

For this approximation, the assumption has been used that the different mass eigenstates of which the initial state is composed have the same momentum p. The approximation yields

$$\delta_{ij} = \frac{\Delta m_{ij}^2}{4E} , \tag{2.14}$$

where $E \simeq p$ is the energy for $m = 0$ and, $\Delta m_{ij}^2 = m_i^2 - m_j^2$. Moreover, we can replace the time t in eq. (2.11) by the baseline L. One reason for that is that the neutrino wave packet is very short compared to every other length of interest. Therefore, the neutrino can be considered to be point-like. The other reason is that neutrinos are highly relativistic so their speed is close to one. Its deviation from one can be neglected.

In the two-flavour case, the indices will often be omitted and Δm^2 and δ will be used for the relevant mass squared splitting and one half of the energy splitting. With the help of this we can rewrite $P_{\nu_e \to \nu_x}(t)$. Note that the energies of the different mass eigenstates read

$$E_i = \frac{E_1 + E_2}{2} \pm \delta_{21} \,, \tag{2.15}$$

where the $+$ corresponds to E_2 and the $-$ to E_1. The factor $\frac{E_2+E_1}{2}$ can now be factored out. It drops out when the square modulus of the transition amplitude is taken.

This step can also be done at an earlier stage of the calculation by subtracting $\frac{1}{2} tr(\mathcal{H}) \mathbb{1}$ from the Hamiltonian. This calculation makes the Hamiltonian traceless. It is valid as it corresponds to multiplying the state vector of the neutrino by a phase. This phase is common to all flavours and does not affect the results of neutrino oscillations. In the following, the traceless form of the Hamiltonian,

$$\mathcal{H} = U diag(-\delta, \, \delta) U^\dagger \,, \tag{2.16}$$

will be utilized frequently.

Eventually, after taking the square modulus of the transition amplitude, the oscillation probability reads (see, e.g. [23])

$$P_{\nu_e \to \nu_x}(t) = \sin^2 2\theta_0 \sin^2(\delta \cdot L) \,. \tag{2.17}$$

2.2 The evolution matrix formalism

A very elegant way to deal with neutrino oscillations is the evolution matrix formalism. It provides a possibility to solve some more complicated equations in a convenient way. The most important reason to use this formalism, however, is its independence of the initial state. Due to that the calculations do not need to be repeated for every new initial state. This formalism, especially the various properties of the evolution matrix, is presented in this section. The calculations follow [24]

for the most part while some of the properties of the evolution matrix are discussed in [25].

The evolution matrix $S(t, t_0)$ is the matrix that describes the time development of the neutrino state,

$$|\nu(t)\rangle = S(t, t_0)\,|\nu(t_0)\rangle\ , \tag{2.18}$$

with the initial condition

$$S(t_0, t_0) = \mathbb{1}\,. \tag{2.19}$$

Inserting eq. (2.18) into eq. (2.1) gives

$$i\frac{d}{dt}S(t, t_0)\,|\nu(t_0)\rangle = \mathcal{H}S(t, t_0)\,|\nu(t_0)\rangle\ . \tag{2.20}$$

This equation should hold for any initial state $|\nu(t_0)\rangle$. Thus,

$$i\frac{d}{dt}S(t, t_0) = \mathcal{H}S(t, t_0) \tag{2.21}$$

should hold. As we see, $S(t, t_0)$ follows the same time evolution equation as $\nu(t)$. Replacing the time t by the baseline L as in the previous section, the evolution matrix reads

$$S(t, t_0) = S(L, L_0) = U diag\left(e^{-iE_1(L-L_0)}, e^{-iE_2(L-L_0)}, e^{-iE_3(L-L_0)}\right) U^\dagger \tag{2.22}$$

Using the traceless form of the Hamiltonian as introduced in eq. (2.16), the explicit form of S in the two-flavour case can be written as

$$\begin{gathered} S(t, t_0) = \begin{pmatrix} \cos\Delta^{'} + ic_{20}\sin\Delta^{'} & -is_{20}\sin\Delta^{'} \\ -is_{20}\sin\Delta^{'} & \cos\Delta^{'} - ic_{20}\sin\Delta^{'} \end{pmatrix} \\ c_{20} = \cos 2\theta_0,\ s_{20} = \sin 2\theta_0,\ \Delta^{'} = \frac{\Delta m^2}{4E}(L - L_0)\,. \end{gathered} \tag{2.23}$$

Once this matrix is known, it is straightforward to compute the oscil-

lation probability $P_{\nu_a \to \nu_b}(L)$:

$$\begin{aligned} P_{\nu_a \to \nu_b}(L) &= |\, \langle \nu_b \,|\, S(L, L_0)\nu(L_0) \rangle \,|^2 \\ &= |\, \langle \nu_b \,|\, S(L, L_0)\nu_a \rangle \,|^2 \\ &= |[S(L, L_0)]_{ba}|^2 \,. \end{aligned} \tag{2.24}$$

The evolution matrix has some useful features which are listed below.

From the definition of the evolution matrix it can be seen that evolution matrices from L_0 to L can always be split into a product of intermediate evolution matrices

$$S(L, L_0) = S(L, L_1)S(L_1, L_0) \,, \tag{2.25}$$

where $L_0 < L_1 < L$.

Assuming there is no absorption or decay of the neutrino and summed over all flavours, the total probability to find the neutrino always remains 1. Therefore, S has to be unitary:

$$S(L, L_0)S(L, L_0)^\dagger = \mathbb{1} \,. \tag{2.26}$$

There are different suitable ways to write $S(L, L_0)$, especially in the approximation of two flavours. One way is to employ the Pauli matrices in the flavour space. The evolution matrix $S(L, L_0)$ for the traceless Hamiltonian can be written as

$$S = Y\mathbb{1} - i\boldsymbol{\sigma}\boldsymbol{X} \,, \tag{2.27}$$

where $\boldsymbol{\sigma}$ is the vector of Pauli matrices and Y and $\mathbf{X}$ are real parameters (see, e.g., [24]). Y and the 3-vector $\mathbf{X}$ now characterize the evolution matrix. They need to be determined by solving eq. (2.21). Due to the

unitarity of S, they fulfil the condition

$$Y^2 + |\mathbf{X}|^2 = 1\,. \tag{2.28}$$

Taking this into account, there is another appropriate way to write the evolution matrix,

$$S = \exp\left[-i\left(\boldsymbol{\sigma}\frac{\boldsymbol{X}}{|\boldsymbol{X}|}\right)\Phi\right]\,, \tag{2.29}$$

where

$$\Phi = \arccos Y = \arcsin(|\mathbf{X}|)\,. \tag{2.30}$$

This parametrization will prove especially useful in the case of a periodic matter profile (see, e.g., [24]).

Due to the unitarity of $S(L, L_0)$, in the two-flavour approximation,

$$P_{\nu_a\to\nu_b}(L) = P_{\nu_b\to\nu_a}(L) \tag{2.31}$$

holds. This is independent of the matter density profile of the setup. For the vacuum case, this can be seen immediately from eq. (2.23).

3 Matter effects in neutrino oscillations

The thesis will cover different matter effects. They are a key to different enhancements of neutrino oscillations. Three of them will be dealt within this thesis. To get an overview of this topic, this chapter comprises a general description of matter effects for two flavour oscillations. The descriptions given in this chapter can be found in [26–28].

3.1 How matter affects neutrino oscillations

When neutrinos fly through matter, they can interact with the particles by weak interaction. To be precise, they can be absorbed or scattered in a way that changes their momentum and energy. The effective potential of such an interaction is of the second order in the Fermi constant

G_F. In this case, the probabilities for the scattering with different particles have to be added. As the Fermi constant is very small, the effect of those interactions can be neglected in most cases. However, the neutrino can also experience elastic forward scattering. This process leaves the momentum unchanged. The contributions of scattering processes on different particles to the effective portential add coherently. Instead of the probabilities, the amplitudes must be added in this case. Thus, the effect is of the first order of G_F. This is still small compared to the energy, but it can be of the size of the energy splitting. Therefore, it can have strong effects on neutrino oscillations (see, e.g. [26]).

Due to the composition of normal matter, the interactions with matter include neutral current (NC) interactions of all flavours via Z^0 exchange, but also charged current (CC) interactions of electron neutrinos with electrons via $W^{\pm}$ boson exchange.

The task is to calculate the effective potential of the weak interactions of neutrinos with matter. Still, the contributions of forward scattering are much larger than the contributions from other interactions. Thus, it is necessary only to calculate the effective potential of forward scattering (see, e.g., [26]).

Therefore, the effective Hamiltonian of the corresponding weak interaction process is written down. The parameters that describe the neutrino such as its energy and momentum are then fixed while integrating over all parameters of the scatterer. Finally, we assume that the matter is unpolarized and has zero total momentum. The result for the CC interactions of the electron neutrino is [6]

$$V_{CC} = \sqrt{2} G_F N_e \,. \tag{3.1}$$

Here N_e is the electron number density in the medium.

If the medium is electrically neutral, the numbers of electrons and protons are the same. Their contributions to the NC effective potential

cancel each other out. Hence, the effective potential for the neutral current reads [6]

$$V_{NC} = -G_F \frac{N_n}{\sqrt{2}}\,. \tag{3.2}$$

However, the NC effective potential is the same for all flavours, except for small radiative corrections. Thus it does not contribute to the change of the flavour state in the oscillation. It can be omitted as long as a sterile neutrino species is not taken into consideration (see, e.g. [27]).

The effective CC potential is then added to the Hamiltonian in eq. (2.1). As the electron density can vary along the path of flight of the neutrino, this makes the Hamiltonian time-dependent. Consequently the Schrödinger equation for neutrino oscillations is in general not analytically solvable. In the following, it will be shown how this new Schrödinger equation can be solved for two flavours and matter of constant density.

3.2 Oscillation of two flavours in constant density matter

As mentioned before, in matter eq. (2.1) has to be changed to [6] (see also [28])

$$i\frac{d}{dt}\left|\nu(t)\right\rangle = \left(\begin{pmatrix} -c_{20}\delta & s_{20}\delta \\ s_{20}\delta & c_{20}\delta \end{pmatrix} + \begin{pmatrix} \sqrt{2}G_F N_e(t) & 0 \\ 0 & 0 \end{pmatrix}\right)\left|\nu(t)\right\rangle\,. \tag{3.3}$$

Here, we have omitted the mean kinetic energy of the two mass eigenstates. That corresponds to using the traceless vacuum Hamiltonian as introduced in chapter 2.1. In addition, the NC potential has been omitted. The notation of chapter 2.1 will be used in the following.

Next, we make the new Hamiltonian traceless like the one in vacuum. Assuming that the matter density is constant, the system is easy to solve with a little trick: If $\mathcal{H}$ does not depend on time, there is one basis, independent of t, in which it is diagonal. If there is such a basis, there is a rotation matrix U_m that connects the flavour and

matter eigenstates. The task now is to find the rotation matrix and the eigenvalues of the diagonalized Hamiltonian. The rest is just analogous to the calculations in vacuum. We can use the vacuum results, for example the evolution matrix, and replace the vacuum mixing angle θ_0 by the mixing angle in matter and the eigenvalues of the traceless vacuum Hamiltonian, $\pm\delta$, by the eigenvalues of the new Hamiltonian, $\pm\omega$.

Denoting the mixing angle in matter by θ_m, these quantities are given by [6, 7]

$$\tan 2\theta_m = \frac{2s_{20}\delta}{2c_{20}\delta - 2V} \tag{3.4}$$

$$\omega = \sqrt{(c_{20}\delta - V)^2 + (s_{20}\delta)^2} \tag{3.5}$$

Here, V is one half of the effective potential V_{CC},

$$V = \frac{G_F N_e}{\sqrt{2}}\,. \tag{3.6}$$

Eq. (3.4) can also be rewritten in the form of the sine of $2\theta_m$ [6, 7],

$$\sin 2\theta_m = \frac{s_{20}\delta}{\sqrt{(c_{20}\delta - V)^2 + (s_{20}\delta)^2}}\,. \tag{3.7}$$

This formulation makes it more obvious that the depth of neutrino oscillations $\sin^2 2\theta_m$ as a function of V has the form of a resonance curve: For very small V, it takes the form of the vacuum mixing. At the resonance,

$$V = \cos 2\theta_0 \delta\,, \tag{3.8}$$

$\sin^2 2\theta_m$ is equal to 1, the depth of mixing is maximal. For very large values of V, it decreases to zero, and mixing is strongly suppressed. In this case, the mixing angle approaches $\frac{\pi}{2}$. The enhancement of neutrino oscillations by matter for a certain relation between $\delta \cos 2\theta_0$ and the effective potential V is part of the so-called MSW resonance effect [6, 7].

3.3 Parametric resonance of neutrino oscillations in matter with a step function profile

Most of the effects examined in this thesis are based on the parametric resonance of neutrino oscillations in a certain type of matter profile called "castle-wall profile" [24]. This section presents the basic features and calculations for this kind of profile and explains the effect of parametric resonance. It follows the calculations in [24]. For a different approach to the parametric resonance see also [10].

The evolution matrix for a baseline in matter of constant density is described by eq. (2.23), but with the effective mixing angle and energy splitting in matter. The evolution matrix for two layers of matter with different constant densities is then given by the product of two of those matrices,

$$S(L,0) \equiv S = S_2(L,L_1)S_1(L_1,0)\,, \tag{3.9}$$

where $S_1(L_1,0)$ and $S_2(L,L_1)$ are the evolution matrices in the first and second layer respectively and S is the evolution matrix over both layers. Here, L_1 is the length of the first layer and $L = L_1 + L_2$ is the length of both layers together.

Now the parameters Y and $\mathbf{X}$ can be calculated for S. They are needed for the parametrization as in eq. (2.27) or eq. (2.29). Multiplying the matrices S_1 and S_2 yields [24]

$$Y = c_1c_2 - s_1s_2(\cos 2\theta_1 \cos 2\theta_2 + \sin 2\theta_1 \sin 2\theta_2)\,, \tag{3.10}$$

$$X_1 = s_1c_2 \sin 2\theta_1 + s_2c_1 \sin 2\theta_2\,, \tag{3.11}$$

$$X_2 = (\sin 2\theta_2 \cos 2\theta_1 - \sin 2\theta_1 \cos 2\theta_2)\, s_1s_2\,, \tag{3.12}$$

$$X_3 = -\left(\cos 2\theta_1 s_1c_2 + \cos 2\theta_2 s_2c_1\right)\,. \tag{3.13}$$

In this case, the notation $\theta_i = \theta_m(V_i)$ has been utilized for the effective mixing angle in the ith layer. $s_i = \sin \omega_i L_i$, $c_i = \cos \omega_i L_i$ have been used for the time-dependent part of the oscillation probabilities where ω_i represents one half of the effective neutrino energy splitting in the

ith layer and L_i its length. This notation will be applied frequently when dealing with such two-layer profiles.

If this two-layer structure is repeated many times, the resulting matter profile is the "castle wall" density profile. Now, the evolution matrix for n periods of this profile, S_n, is achieved by taking S to the power n. This can be implemented with the parametrization of eq. (2.29):

$$S(nL, 0) \equiv S_n = \exp\left[-i\left(\boldsymbol{\sigma}\frac{\boldsymbol{X}}{|\boldsymbol{X}|}\right)n\Phi\right] . \tag{3.14}$$

From this, a few steps of calculation show S_n in a very helpful way:

$$S_n = \cos n\Phi\, \mathbb{1} - i\frac{\boldsymbol{\sigma}\boldsymbol{X}}{|\boldsymbol{X}|}\sin n\Phi \tag{3.15}$$

This form is especially convenient for calculating the transition probability

$$P_{\nu_e\to\nu_x}(nL) = |[S_n]_{xe}]|^2 \tag{3.16}$$

$$= \frac{|X_2 \sin n\Phi - iX_1 \sin n\Phi|^2}{|\boldsymbol{X}|^2} \tag{3.17}$$

$$= \frac{X_1^2 + X_2^2}{X_1^2 + X_2^2 + X_3^2}\sin^2 n\Phi\,. \tag{3.18}$$

Just as in the case of vacuum oscillations, this probability factorizes into an amplitude which is independent of L and an oscillation part that contains the L-dependence. As in the case of constant density, the prefactor can be maximized. This will lead to oscillations with maximal depth. The condition for this is

$$X_3^2 = (\cos 2\theta_1 s_1 c_2 + \cos 2\theta_2 s_2 c_1)^2 = 0\,. \tag{3.19}$$

This condition is called the resonance condition [24]. There are different ways of fulfilling it, but the applied one is

$$c_1 = c_2 = 0\,. \tag{3.20}$$

In this case,

$$\Phi = 2\theta_2 - 2\theta_1 \tag{3.21}$$

and the oscillation probability is given by [24]

$$P_{\nu_e \to \nu_x}(nL) = \sin^2 \left[2n(\theta_2 - \theta_1)\right] . \tag{3.22}$$

4 Parametric resonance in an artificial density profile

In the previous section, the parametric resonance of neutrino oscillations in matter with a "castle-wall" density profile was discussed, and eq. (3.22) has been derived. This enhancement of neutrino oscillations via parametric resonance has not yet been observed in experiment. One can consider different setups to test it. One method is the measurement of atmospheric neutrinos passing through the core of the earth. This might be the most promising way to probe parametric enhancement of neutrino oscillations [29]. Chapter 5 will discuss the resonance in the core of the earth for neutrinos from a neutrino factory.

Another possible setup would be to build or find a baseline that has a "castle-wall" density profile. Such a setup might keep the baseline short while showing parametric enhancement of neutrino oscillations. The limits of such an experiment will be explored in the following chapter. It will turn out that such an experiment is not feasible.

A simplification of the three-flavour approach to study the oscillation probability is to apply perturbation theory of zeroth order in $\frac{\Delta m^2_{21}}{\Delta m^2_{31}}$. In this approach, one of the neutrino flavours can be decoupled from the other two by a rotation in the μ-τ subspace of the flavour space by the angle θ_{23} [25]. Hence, the calculation is reduced to two flavours, e and x. Here, x is the combination of μ and τ produced by the rotation of the μ-τ subspace. As a result of the reduction to two flavours there is only one independent oscillation probability. The equation

$$P_{\nu_e \to \nu_e} = 1 - P_{\nu_e \to \nu_x} \tag{4.1}$$

can be applied to deduce the other probabilities. The transition probabilities in the flavour basis e, μ and τ are recovered by multiplying $P_{\nu_e \to \nu_x}$ with c_{23}^2 or s_{23}^2 [29]. $P_{\nu_e \to \nu_x}$ will be employed as the oscillation probability in the following analysis. Besides the advantages discussed above, it is directly influenced by matter effects because it contains electron neutrinos as the initial flavour.

In this chapter, a strongly idealized version of a neutrino experiment is utilized. It will be assumed that the neutrino oscillation parameters are known with an accuracy of less than one percent. In addition to that, the sensitivity of the detector for the oscillation probability is presumed to be at the order of permille. Moreover, the neutrino beam is supposed to be monochromatic. These are quite unrealistic assumptions. Especially a monochromatic neutrino beam will not be feasible in neutrino beam experiments. But if the studied experiment is not feasible under this idealized assumptions, it will not be feasible under realistic conditions. The reasons behind will be discussed later. Thus, this idealized version of a neutrino experiment can help to demonstrate that a neutrino experiment with an artificial density profile can not be used to observe parametric enhancement of neutrino oscillations.

To determine whether such an experiment with an artificial matter density profile can be done, there are different aspects to consider. The first one is the objective to be achieved. It has to be clear which quantity shall be measured and to what extend the experiment is sensitive to this quantity. The second aspect is the constraints of the experiment. It has to be defined which parameters are constrained and what size they can take.

Concerning the first aspect, the measured quantity is the parametric enhancement of the oscillation probability. Therefore, the parametrically enhanced oscillation probability, P_{pr} should be distinguishable from the normal neutrino oscillation probability in matter of constant density, P_{cd}. This means, P_{pr} should be bigger than the expected value of the oscillation probability in matter with the constant density

$\bar{\rho} = \frac{\rho_1 L_1}{L} + \frac{\rho_2 L_2}{L}$. In the present case, $\bar{\rho}$ is approximated by $\bar{\rho} \simeq \frac{\rho_1 + \rho_2}{2}$. It will be shown later that the end of each period of the matter density profile approximately coincides with a minimum of P_{cd}.

As a result, the difference between P_{pr} and P_{cd}, called ΔP, can be approximated by the difference between P_{pr} and zero, P_{min}. Thus, the oscillation probability in the artificial density profile setup must be large enough to be distinguished from zero. However, a slight deviation of P_{cd} from the minimum after one period can accumulate over a large number of periods. This is why the minimal oscillation probability should not be chosen too small. As an optimistic assumption the minimal parametric enhanced oscillation probability $P_{min} = 0.01$ is selected.

The second aspect concerns the constrains on our parameters. There are different limitations to experiments on the earth. Firstly, the density of matter in the earth is, at least for the use of an experiment, limited by about $10\,\mathrm{g/cm^3}$. For many setups the maximal density is even lower. Secondly, the baseline of the experiment can not be chosen arbitrarily long. According to the setup, limits may come from the earth diameter, the flux of the neutrino source and the $\frac{1}{L^2}$-dependence of the flux or just the maximal size of an artificial density profile. The third limit is the one that will be applied in this section. Nevertheless the possibility of a beamline which accidentally has the desired matter profile because of mountains or hills is taken into account.

The next step is combining both aspects, the requirement of the result and the limits on the parameters. Thereto, the question has to be answered whether P_{min} can be reached within the limits of our experimental parameters. For testing, a measured oscillation probability of P_{min} is assumed. Then all parameters except one are set to convenient values within the allowed domain. Finally, the requirements for the last parameter are computed and compared to the restrictions of this parameter. In this case, it will be determined how long the baseline must be to reach P_{min}. It will be shown that the required baseline of an artificial profile is too long to be built. Furthermore, there is no chance

to find one accidentally. This result will turn out to be independent of the neutrino energy to the first order in the used approximation.

4.1 Analytical study

To understand certain effects such as resonances it is often helpful to analyse approximate solutions of the problem. Their properties sometimes show interesting features hard to understand by numerical calculation. To analyse the present case, the starting point is the transition probability at resonance for a "castle-wall" density profile as given by eq. (3.22).

Demanding that the probability takes a certain value P_{min}, it is possible to calculate the number n of layers needed. n is given by the integer that is closest to

$$\frac{\arcsin(\sqrt{P_{min}})}{2|\theta_2 - \theta_1|} \,. \tag{4.2}$$

This derives directly from eq. (3.22). This formula has a few interesting characteristics. As expected, the number of layers depends on the difference of the mixing angles. The larger the difference, the smaller n needs to be. The difference, however, can not become arbitrarily large. The maximal difference that can be achieved is $\frac{\pi}{2} - \theta_0$ [4] . It corresponds to infinite density in one and vacuum in another layer. Note that n can only take integer values, as mentioned above. If the oscillation probability for a baseline with an incomplete layer in the end is calculated, a different evolution matrix has to be used [24].

The next interesting characteristic of this formula is the proportionality to arcsin of $\sqrt{P_{min}}$. For small values of P_{min}, such as 10^{-2}, this can be approximated as $\sqrt{P_{min}}$. As a result of this dependence n can only be lowered by a factor of $\sqrt{10}$ if P_{min} can be lowered by an order of magnitude. In addition to that, the deviation of P_{cd} from zero represents a lower bound for P_{min}. Taking both into account, the pro-

[4] The mixing angle can be chosen to lie between 0 and $\frac{\pi}{2}$ by rephasing of the neutrino fields. See [30].

portionality to $\sqrt{P_{min}}$ and the lower bound from P_{cd}, the benefit from an increase of experimental sensitivity on the length of the baseline is limited.

The total length of the baseline, L, is not only determined by the number of layers, but also by their size:

$$L = n(L_1 + L_2)\,, \tag{4.3}$$

where L_1 and L_2 are the lengths of the single layers. They are determined by the resonance condition as given in eq. (3.20). In terms of the oscillation phase, the resonance condition can be written in the form

$$\omega_i L_i = \frac{\pi}{2} + k_i\pi, \qquad k_i \in \mathbb{N}\,. \tag{4.4}$$

The calculations are restricted to $k_i = 0$ for now, because this is the condition with the shortest length of a single layer. In this case, the length of each layer is given by

$$L_i = \frac{\pi}{2\omega_i}\,. \tag{4.5}$$

Here, we see that the length of every period of the profile corresponds approximately to an oscillation phase of π . As a result, the oscillation probability in matter of the constant density $\bar{\rho}$ will be close to the oscillation minimum at that point [5] . Thus, this oscillation probability vanishes at the end of each period of the density profile. Therefore, we can compare P_{pr} to zero.

The length of the individual layers depends only on the effective neutrino energy splitting. Nonetheless, neither the vacuum mixing angles nor the mass splitting are adjustable parameters of a potential experiment, in contrast to the energy E as defined in chapter (2.1). Thus, it could be of interest to see the energy dependence of the to-

[5]Note that this is only valid because of the assumption that the neutrino beam is monochromatic. For other energies than the one used to calculate L, P_{cd} might be much larger and P_{pr} is not at the resonance. A numerical discussion on that topic can be found in the next section.

tal required baseline. Without any approximations, this dependence is rather complex. However, the problem contains a small parameter, $\frac{V_i}{\delta}$ [6]. An expansion in this parameter will simplify the calculations significantly. The following example shows that this parameter indeed is small in the present case.

The matter density is assumed to be about $\rho = 2.8 \frac{g}{cm^3}$, which is the density of the earth crust. Per nucleon, we assume $Y_e = 0.5$ electrons, as the numbers of neutrons and protons in the earth are approximately equal, while the number of protons and electrons are exactly equal. We also use $\hbar c$ in the units of length times energy as given by the Particle Data Group [31],

$$\hbar c = 1.973\,269\,788 \times 10^{-5}\,\mathrm{eV\,cm}\,. \tag{4.6}$$

The Fermi constant has the value [31]

$$G_F = 1.166\,378\,7 \times 10^{-5}\,\mathrm{GeV}^{-2}(\hbar c)^3 \tag{4.7}$$

and the Avogadro constant is [31]

$$N_A = 6.022\,140\,857 \times 10^{23}\,\mathrm{mol}^{-1}\,. \tag{4.8}$$

With the help of these quantities we can now calculate the effective potential in the earth crust, V_c

$$V_c = \frac{G_F}{\sqrt{2}} N_A \rho Y_e = 3.816\,23 \times 10^{-14}\,\rho Y_e = 5.34 \times 10^{-14}\,\mathrm{eV}\,. \tag{4.9}$$

The other value of interest is δ. The oscillation channel we chose is mediated by the $1-3$-mixing angle and mass squared splitting. Therefore, the relevant mass splitting in the present case is

$$\Delta m^2 = \Delta m^2_{31} = \left(2.457^{+0.047}_{-0.047}\right)\,10^{-3}\mathrm{eV}^2\,. \tag{4.10}$$

[6] There are actually two parameters, $\frac{V_1}{\delta}$ and $\frac{V_2}{\delta}$, but as L_i and ω_i are expand, each expansion will be in only one of them. In the final formula, their sum and difference will appear, so that there are strictly speaking two corrections in the first order, one for each parameter.

This is the global fit best value and 1σ range at the moment [11]. Now taking the best fit value of Δm^2_{31} and using eq. (2.14), δ is easy to calculate:

$$\delta = 6.1425 \times 10^{-10} \frac{\text{eV}}{E(\text{MeV})} \,. \tag{4.11}$$

Accordingly, $\frac{V_c}{\delta}$ takes the value

$$\frac{V_c}{\delta} = 8.6980 \times 10^{-5}\, E(\text{MeV}) \,. \tag{4.12}$$

As revealed, in the MeV energy rang, this quantity is small enough to be utilized as an expansion parameter.

The first quantity to be developed is one half of the effective energy splitting as given in eq. (3.5). It can be rewritten in the convenient form

$$\omega_i = \delta \sqrt{1 + \left(\frac{V_i}{\delta}\right)^2 - 2c_{20}\frac{V_i}{\delta}} \,. \tag{4.13}$$

A Taylor expansion of ω_i to linear terms in $\dfrac{V_i}{\delta}$ yields

$$\omega_i \simeq \delta - c_{20} V_i \,. \tag{4.14}$$

Inserting this into eq. (4.5) and again linearising by Taylor expansion, L_i at the parametric resonance takes the form

$$L_i \simeq \frac{\pi}{2\delta}\left(1 + c_{20}\frac{V_i}{\delta}\right) \,. \tag{4.15}$$

To 0th order in the expansion parameter L_i is proportional to the neutrino energy, while the first order correction is quadratic in E. In order to keep the length of each layer short, the energy should not be too large. E is assumed to be around a few MeV, but it could as well be up to 1-2 GeV.

The next step is linearising the effective mixing angles in matter by Taylor expansion. Therefore eq. (3.7) and the linearised form of ω_i are

used:

$$\begin{aligned}\theta_i &= 0.5 \arcsin\left(\frac{\delta}{\omega_i} s_{20}\right) \\ &\simeq \theta_0 + 0.5 s_{20} \frac{V_i}{\delta}\end{aligned} \tag{4.16}$$

Now, this formula and the simplified form of L_i can be combined. The result is a formula for the total baseline length:

$$\begin{aligned}L &\approx \frac{\pi}{2\delta}\left(2 + c_{20}\frac{V_1+V_2}{\delta}\right)\frac{\delta \arcsin\left(\sqrt{P_{min}}\right)}{s_{20}|V_2 - V_1|} \\ &= \frac{\pi \arcsin\left(\sqrt{P_{min}}\right)}{s_{20}|V_2 - V_1|} + \frac{\pi c_{20} \arcsin\left(\sqrt{P_{min}}\right)(V_1+V_2)}{2\delta s_{20}|V_2 - V_1|}\end{aligned} \tag{4.17}$$

This is one of the main results of this analysis. The first term on the right side is independent of δ. Therefore, it is independent of the neutrino energy. As a result, as long as $\frac{V}{\delta}$ is very small, the length of the baseline that is needed to get a certain size of oscillation probability will not change with energy.

The dependence of L on P_{min} is the same as for n. The properties of that dependence have been described above. The most important result disclosed that n does not depend on P_{min} very strongly. Moreover P_{min} should not become smaller than P_{cd}. Combining the dependencies on E and P_{min} of the leading term of L it is revealed that L can not be shortened significantly by increasing the accuracy of the experiment or lowering the neutrino energy.

Both terms, the first and the second one on the right of eq. (4.17), are proportional to $|V_2 - V_1|^{-1}$. If the difference of the effective potentials is small, this is a strong dependence. However, the effective potentials are the most strictly limited parameters as the maximal density of earth matter can not be raised. Hence, the strong dependence on the difference of the matter densities can not be applied to shorten L significantly.

The second term is of the first order in the small parameter. This term has an additional factor of $c_{20}\frac{V_1+V_2}{2\delta}$. If $V_1 \simeq 0$, $V_2 - V_1 \simeq V_2 + V_1$. As a result, this term is independent of the density of the second layer as long as $V_1 \simeq 0$. The term is proportional to E because it contains a factor of δ^{-1}. As a result this term will rise linearly with energy. This is rather problematic than helpful, as the correction is positive, and will even increase L. Anyway, for small energies of a few MeV or less this factor is strongly suppressed compared to the leading order term by $\frac{V_1+V_2}{\delta}$.

This analysis shows that for energies of some MeV the length of the baseline required to reach a given transition probability at the parametric resonance is to the first order independent of the neutrino energy. It is proportional to the square root of the required transition probability. Thus, it will be difficult to reduce the length of the required baseline for such an experiment, even if lower energies can be used and the sensitivity can be increased.

The approximations done here might be valid only for small energies, but higher energies can be excluded for different reasons. As eq. (4.5) shows, L_i grows with E. Indeed, as V_i is limited, ω_i decreases with E. This is why at the GeV-scale, where the validity of the applied approximation reaches its limits, the length of every single layer would be too large to built or find a "castle-wall" density profile. For example, to reach an oscillation phase of $\frac{\pi}{2}$ for a neutrino with an energy of 5 GeV in the crust of the earth, one would need a baseline of

$$L \simeq 4221\,\mathrm{km}\,. \tag{4.18}$$

The remaining question relates to the size of the first term in eq. (4.17). It determines whether the studied experiment can be build to observe the parametric enhancement of neutrino oscillations.

4.2 Numerical estimates

In this section, it is analysed whether the setup with the artificial density profile can be utilized to observe the parametric enhancement of neutrino oscillations or not. Therefore, the length of the required baseline is calculated in the approximation given above.

The assumptions for the calculations will be as follows: The value of the neutrino energy is 5 MeV. The matter profile those neutrinos pass consists of alternating layers of different materials. One of the materials is proposed to be air, so that $V_1 \simeq 0$. The other one is the crust of the earth which means $V_2 = V_c = 5.34 \times 10^{-14}\,\text{eV}$. We assume $P_{min} = 10^{-2}$. The mass squared difference is adopted from the example in the previous section. The mixing angle θ_{13} and its 1σ error are given by [11]

$$\theta_{13} = \left(8.50^{+0.20}_{-0.21}\right)^\circ . \tag{4.19}$$

To get an initial idea, the thicknesses of the individual layers are computed with the help of eq. (4.15). The results for the lengths of the layers are

$$\begin{aligned} L_1 &= \frac{2\pi}{\Delta m^2}\, E(\text{MeV}) \simeq 504.62\,\text{m}\, E(\text{MeV}) \simeq 2523.08\,\text{m}\,, \\ L_2 &= \frac{2\pi}{\Delta m^2}\, E(\text{MeV}) + \frac{8\pi c_{20} V_c}{(\Delta m^2)^2}\, (E(\text{MeV}))^2 \\ &\simeq 504.62\,\text{m}\, E(\text{MeV}) + 0.04\,\text{m}\, (E(\text{MeV}))^2 \simeq 2524.13\,\text{m}\,. \end{aligned} \tag{4.20}$$

In the last line it is clearly visible that the correction of the length of the layers due to matter is quite small. It becomes clear that building an actual matter profile might become difficult, even if n is small, as the length of each layer is already about 2.5 km for the energy of 5 MeV.

Next, the number n of layers is calculated as described in eq. (4.2).

$$n \simeq \frac{\delta \arcsin 0.01}{s_{20} V_c} \simeq 3.939 \times 10^3\, \frac{1}{E(\text{MeV})} \simeq 788 \tag{4.21}$$

Multiplying the two results yields for the total baseline

$$\begin{aligned} L &\simeq 1009.23\,\mathrm{m}\,E(\mathrm{MeV})\,3.939\times10^{3}\,\frac{1}{E(\mathrm{MeV})} \\ &\quad + 0.04\,\mathrm{m}\,E^{2}(\mathrm{MeV}^{2})\,3.939\times10^{3}\,\frac{1}{E(\mathrm{MeV})} \\ &= 3975\,\mathrm{km} + 165\,\mathrm{m}\,E(\mathrm{MeV})\,. \end{aligned} \tag{4.22}$$

This is not a very long baseline for a neutrino oscillation experiment, but it is too long for building the setup described above.

This result is not really surprising. If we go to low energies, matter effects in neutrino oscillations are very tiny. Due to this, many layers, around 800 in this case, are needed to achieve a sizeable oscillation probability. The length of each layer decreases with energy, but it does not become small enough to compensate for the large number of layers needed. Therefore, performing such an experiment successfully requires much higher densities or much longer distances.

One possibility to achieve higher densities is using lead instead of the crust of the earth in the layers with higher density. This will increase the density to [32]

$$\rho_l \simeq 11.35\,\mathrm{g/cm}^3\,. \tag{4.23}$$

Lead has approximately

$$Y_e \simeq 0.4 \tag{4.24}$$

electrons per nucleon. The effective potential in lead as given by eq. (3.8) is

$$V_l \simeq 1.73\times10^{-13}\,\mathrm{eV}\,. \tag{4.25}$$

As a result, the length of the layer in lead is

$$L_2 \simeq 504.62\,\mathrm{m}\,E(\mathrm{MeV}) + 0.14\,\mathrm{m}\,E^{2}(\mathrm{MeV}^{2})\,. \tag{4.26}$$

Eq. (4.15) was applied to derive this result. The number of layers for

the same P_{min} as before is

$$n \simeq 1215 \, [E\,(\mathrm{MeV})]^{-1} \, . \tag{4.27}$$

Eventually, the result for the total baseline is

$$L \simeq 1226\,\mathrm{km} + 165\,\mathrm{m}\, E(\mathrm{MeV}) \tag{4.28}$$

While the second term on the right side is approximately the same as in eq. (4.22), the first one is smaller by about 69%. Anyway, it is still larger than 1000 km. Even when such a dense material as lead is used, a feasible baseline length can not be reached.

To justify the approximation $\Delta P = P_{min} - P_{cd} \simeq P_{min}$, P_{cd} is calculated for the given baseline. The same energy as in the previous calculations is assumed. The effective matter potential is given by

$$\bar{V} = \frac{V_1 + V_2}{2} = \frac{V_c}{2} \, . \tag{4.29}$$

For the baseline the corrections of the first order are included. Using the formulae derived in section (3.2), the result is

$$P_{cd} \simeq 8.9 \times 10^{-10} \, . \tag{4.30}$$

The result shows that it was indeed justified to use P_{min} instead of ΔP. Note that P_{cd} is still small compared to P_{min} for $E = 2\,\mathrm{GeV}$. There

$$P_{cd}(E = 2\,\mathrm{GeV}) \simeq 1.7 \times 10^{-4} \, . \tag{4.31}$$

Thus $\Delta P \simeq P_{min}$ can be applied in the idealized experiment.

However, small deviations from the idealized assumptions will lead to a P_{cd} which is large compared to P_{min}. One example for an idealized assumption is the neutrino energy. The assumption of a monochromatic beam has been the most unrealistic one. A more realistic but still optimistic assumption would be to assume an energy spectrum that spreads 1 MeV above and below the resonance, in this case 5 MeV.

The maximal result for P_{cd} in this energy range is

$$P_{cd} \simeq 0.086 \tag{4.32}$$

at the energy

$$E \simeq 4.33\,\mathrm{MeV}\,. \tag{4.33}$$

Here, the spectrum has been assumed to be constant between 4 and 6 MeV. The same formula and baseline are applied as before. Since the result for P_{cd} is eight times larger than P_{min}, P_{cd} will exceed the parametrically enhanced oscillation probability within the range of the spectrum, even if the spectrum is not a step function, but peaks around the resonance energy.

Similar results are achieved if the oscillation parameters θ_{13} and Δm^2_{31} are varied. If we maximize P_{cd} over the allowed 3σ-ranges of θ_{13} and Δm^2_{31}, P_{cd} takes the value

$$P_{cd} \simeq 0.096\,. \tag{4.34}$$

These results show the large impact of the deviations from the idealized assumptions. For a realistic experiment a much larger P_{min} has to be chosen independently of the sensitivity of the experiment. According to the analysis in the previous chapter a constraint on P_{min} introduces a strong lower bound on the required baseline. As a result the required baseline for a realistic experiment is longer than the results acquired in this section. Thus, the calculations with the idealized assumptions are an estimate for the shortest required baseline.

To put it briefly, we can describe the situation of an oscillation experiment that uses a periodic density profile to enhance neutrino oscillations by an expansion of the baseline L in the small parameter $\frac{V}{\delta}$. The leading term of this expansion is independent of the energy E. Therefore, there is a strong lower bound to the length of such an experiment. Numerical calculations show that this minimal baseline is already too long to create a periodic step function matter structure for

the whole baseline. This experiment is thus not useful to observe the parametric enhancement of neutrino oscillations.

5 Parametric resonance of oscillations of neutrinos traversing the core of the earth

In the last few years, huge progress in the determination of θ_{13} has been made. It is now known that it is non-zero, and, moreover, relatively large. In this context, the discussion on long baseline neutrino experiments will be taken up again in this chapter. In particular, the proposal of the authors of [33–35] to send a neutrino beam through the core of the earth will be discussed. This study focuses on the question, whether it will be possible to observe the parametric enhancement of neutrino oscillations by such an experiment.

The earth density profile can roughly be described by two regions of constant density: The core with a radius of $r = 3485\,\mathrm{km}$ [36] and an average density of $\rho_c \simeq 11.5\,\mathrm{g/cm^3}$, and the mantle with an average density of $\rho_m \simeq 4.5\,\mathrm{g/cm^3}$. A baseline passing through the core of the earth thus has a "castle wall" density profile with 3 layers. For this reason, oscillations of neutrinos traversing the core of the earth can experience parametric enhancement. For $\sin^2 2\theta_{13} \simeq 0.1$, the parametric enhancement is one of the strongest enhancements of neutrino oscillations for neutrinos going through the earth [29].

However, the corresponding baseline is very long and a lot of flux of a beam will be lost on the way. This will lead to decreased statistics. A large detector can be utilized to compensate for the loss of flux. The authors of [33] propose a feasible solution. The planned upgrade of the neutrino telescope IceCube called PINGU (Precision IceCube Next Generation Upgrade) [37] could be used as a Mt-size detector. Moreover, there are several neutrino facilities in the northern hemisphere that could serve as a source for such an experiment.

The discussion on sending a neutrino beam to PINGU will be up-

dated with the measured value of θ_{13}, and recent estimates of the sensitivity of the PINGU detector. The results of the latest global fits for θ_{13} will be used as priors in the calculation. The calculation will be carried out for both, normal and inverted neutrino mass ordering and the according best fit values for the neutrino oscillation parameters. In the calculation, the parametric resonance of neutrinos passing the core of the earth will be emphasized. It will be tested for which energy resolution the experiment is sensitive to the parametric enhancement of neutrino oscillations. The reach for the oscillation parameters such as the mass hierarchy, or for the density of the earth core, has been studied widely [33, 34, 38, 39]. The GLoBES software [40, 41] will be used as a tool for simulation and calculation.

5.1 Preliminary considerations: oscillation probabilities

Before calculating the experimental results, the oscillation probabilities for the observed channels will be determined. They provide first information on the expected energy spectrum for a certain detected neutrino flavour. For neutrino oscillations inside the earth an interplay of MSW-resonances and parametric resonances takes place, leading to a strong enhancement of neutrino oscillations for energies between 2 and 10 GeV [29, 33]. The interplay of the different resonances makes it difficult to find a setup that differs from the present one only by the parametric resonance. If the average density of the baseline is utilized instead of three layers, not only the parametric resonance disappears, but the two MSW-resonances will become one single MSW-resonance. However, the comparison between the setup with three layers and the one with averaged density can serve as a first test for the observability of the parametric resonance. Hence, the results of the calculations will be compared to the results obtained with an average-density setup.

All of the neutrino sources in the northern hemisphere have approximately the same distance to PINGU: $L \simeq 12\,000\,\text{km}$. This corresponds to a nadir angle of $\theta_n \simeq 20°$. Here the facility with the longest baseline is used. The chosen facility is the Rutherford Appleton Laboratory (RAL) in the United Kingdom, and the length of the baseline is

$L \simeq 12\,020\,\mathrm{km}$. The average density in the mantle and in the core are calculated with the preliminary earth model (PREM) [42]. The result is shown in fig. 1. It is similar to the matter density profile used in [33].

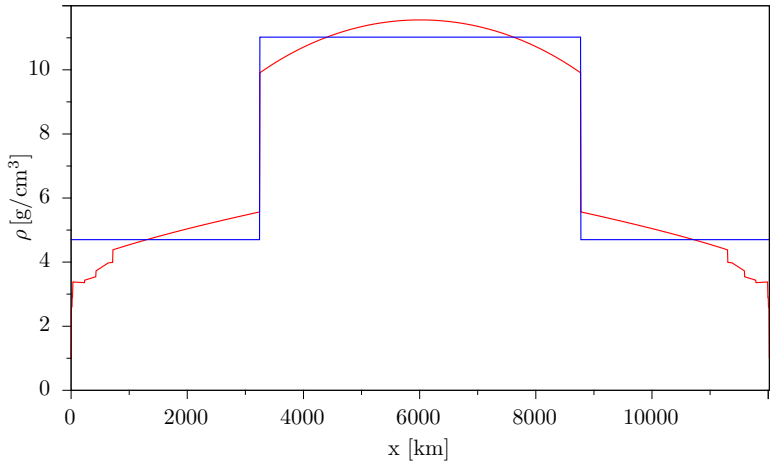

Figure 1: *Earth matter density profile for a baseline of* $L = 12\,020\,\mathrm{km}$. *Red line: PREM matter profile [42], blue line: three-layer approximation.*

In this setup, the neutrino source will be a neutrino factory [43]. In a neutrino factory, muons with positive or negative charge are produced and stored in a muon storage ring. Those muons eventually decay:

$$\begin{aligned} \mu^- &\to \nu_\mu\, e^-\, \bar{\nu}_e \\ \mu^+ &\to \bar{\nu}_\mu\, e^+\, \nu_e\,. \end{aligned} \tag{5.1}$$

The resulting neutrino beam consists of muon neutrinos and electron antineutrinos, or of muon antineutrinos and electron neutrinos. The oscillation probabilities are calculated for the oscillation channels $\nu_e \to \nu_\mu$ and $\nu_\mu \to \nu_\mu$ for neutrinos and antineutrinos. These are the oscillation channels employed in the experiment. Though other oscillation channels could in principle be observed, these are the ones that are easiest to differentiate from other channels. To avoid misidentification, these channels are chosen as signal.

In fig. 2, the top row displays the oscillation probabilities for the case when μ^+ are stored in the muon storage ring. The bottom row

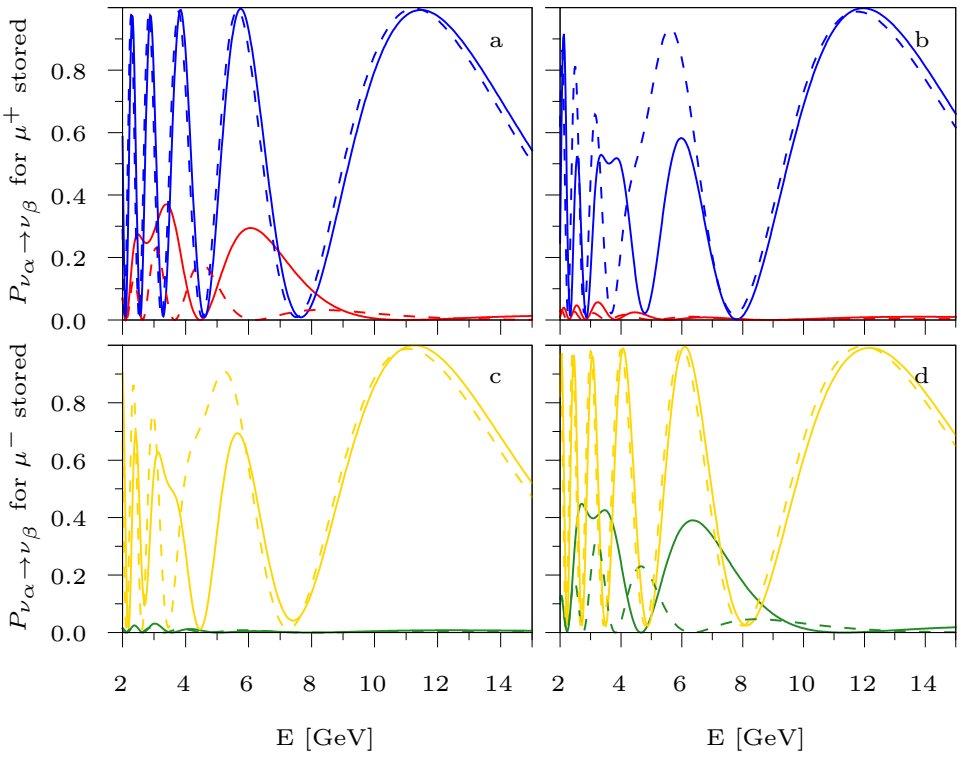

Figure 2: *Oscillation probabilities for the channels $\nu_e \to \nu_\mu$ (red line), $\bar{\nu}_\mu \to \bar{\nu}_\mu$ (blue line), $\nu_\mu \to \nu_\mu$ (yellow line) and $\bar{\nu}_e \to \bar{\nu}_\mu$ (green line). Solid lines: the three-layer approximation of the PREM-profile is assumed. Dashed lines: The averaged density of the RAL-PINGU baseline is applied. Left column: Normal mass ordering is assumed. Right column: Inverted mass ordering is assumed.*

represents the channels for μ^- stored. The solid line has been calculated with the three-layer approximation of the PREM profile. For the dashed lines the average density has been utilized. All calculation use a full three-flavour approach. We see that in each case one of the channels is enhanced by matter: For the normal mass ordering the neutrino channels are enhanced while the antineutrino channels are enhanced in the case of inverted mass ordering.

Besides that, there are only small energy windows in which the muon neutrino disappearance probability (blue or green line) does not dominate. Since the PINGU detector will not have direct charge identification, the muon neutrino disappearance channel can be discrimi-

nated from the muon neutrino appearance channel by the energy resolution [33] [7] or by a statistical discrimination of μ^+ and μ^- based on the different lifetimes of those particles in the detector material [44]. However, the energy resolution is an important experimental parameter for the sensitivity of the experiment to the parametric resonance of neutrino oscillations.

Considering the solid lines in fig. 2, in the $\nu_e \to \nu_\mu$-channel (or the corresponding channel for antineutrinos in the case of inverted mass ordering), we can identify the double peak at 2-4 GeV with the MSW-resonance in the core of the earth (smaller left peak) and the parametric resonance (right peak). The peak around 6-7 GeV is dominated by the MSW-resonance in the mantle [29]. It becomes clear that for this baseline the MSW-resonance in the core and the parametric resonance appear for similar energies, and are difficult to separate. Hence, a high energy resolution is not only needed to distinguish between the two oscillation channels, but to distinguish between the MSW-resonance in the core and the parametric resonance.

The dashed lines show a MSW-resonance between 2 and 6 GeV. It contains three oscillation maxima. However, those maxima do not appear at the same energies as the two MSW-resonances and the parametric resonance in the case of three layers. Furthermore the maxima are smaller and narrower than in the case with three layers. If the energy resolution is high enough to determine the positions of the resonance peaks in the $\nu_e \to \nu_\mu$-channel, it should be possible to observe the parametric resonance of neutrino oscillations.

5.2 Setup of the experiment

Source The energy spectrum of the neutrino factory neutrino beam has a peak close to the energy of the muons and is zero above the

[7] Note that the argument in [33] was done with $\nu_e \to \nu_\mu$ and $\nu_\mu \to \nu_\mu$ instead of $\nu_e \to \nu_\mu$ and $\bar{\nu}_\mu \to \bar{\nu}_\mu$ and for smaller θ_{13}. This leads to wider energy regimes in which the $\nu_e \to \nu_\mu$-channel dominates.

muon energy [45]. The energy of the stored muons in this setup is assumed to be 50 GeV. The energy spectrum of a neutrino factory as given in [45] is shown in fig. (3). It is visible that the flux increases for

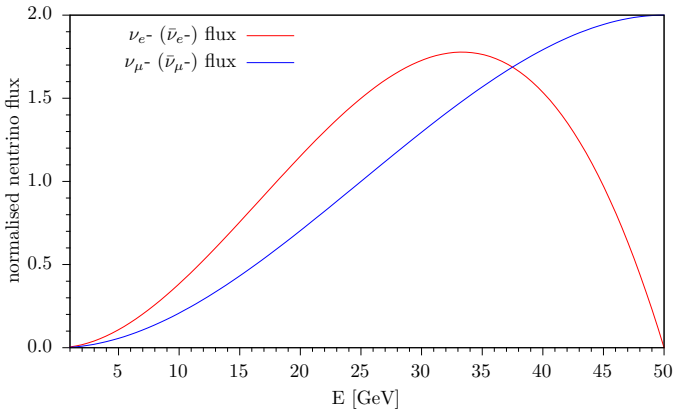

Figure 3: *Normalised energy spectrum of a neutrino beam produced by a neutrino factory as given by eq. (14b) in [45]. The assumed muon energy is* 50 GeV. *Red:* ν_e *or* $\bar{\nu}_e$ *flux. Blue:* ν_μ *or* $\bar{\nu}_\mu$ *flux.*

energies below 35 GeV. At this energy the ν_e-flux reaches a maximum, and starts to decrease, while the ν_μ flux increases further towards the muon energy. 10.66×10^{20} muons are stored per year.

Detector The detector will be the PINGU upgrade of the IceCube neutrino telescope. It is a large Ice Cherenkov detector [46]. It consists of a number of photo-detectors which are embedded into the ice of the south pole. In the volume of the PINGU upgrade, the photo-detectors are separated by about 5 m of ice. This region is located inside the deep, clear ice. It is surrounded by a large region of ice with a lower density of photo-detectors. This larger volume serves as a veto to exclude cosmic ray muons [37]. The considered setup will use the proposed "40-string configuration" [37], where 40 additional strings of photo-detectors are added to the existing IceCube detector. The specifications of the detector will be as follows:

Event misidentification In the detector, the neutrinos can weakly interact and produce their corresponding charged lepton. Those lep-

tons can be observed and identified by the event topology. The tracks of the muons produced in CC interactions are utilized as signal. Other possible topologies are cascade events of NC interactions or CC interactions of other leptons [33]. Considering the flavour composition of the beam, the oscillation channels $\bar{\nu}_e \to \bar{\nu}_\mu$ and $\nu_\mu \to \nu_\mu$ or $\bar{\nu}_\mu \to \bar{\nu}_\mu$ and $\nu_e \to \nu_\mu$ respectively contribute to the signal. As mentioned earlier, those two channels shall be discriminated by the energy resolution.

Channels other than the signal channels are considered background. The channels included in the background are listed in tab. (1) below. It is assumed that 20% of the cascade events are misidentified as muon tracks [39]. Moreover, we assume that 17% of the taus decay into muons, producing an intrinsic muon background [33].

Factor	Background channel
20%	$\bar{\nu}_e \to \bar{\nu}_e$ (NC cascade)
20%	$\nu_\mu \to \nu_\mu$ (NC cascade)
20%	$\bar{\nu}_e \to \bar{\nu}_e$ (CC cascade)
20%	$\nu_\mu \to \nu_e$ (CC cascade)
20%	$\bar{\nu}_e \to \bar{\nu}_\tau$ (CC cascade)
20%	$\nu_\mu \to \nu_\tau$ (CC cascade)
17%	$\bar{\nu}_e \to \bar{\nu}_\tau \to \tau^+ \to \mu^+$ (intrinsic τ count)
17%	$\nu_\mu \to \nu_\tau \to \tau^- \to \mu^-$(intrinsic τ count)

Table 1: *Background channels used in the simulation of the PINGU detector. In the simulation the background rates for each of those channels will be multiplied by the "Factor" and then added to the signal event rate. The background channels are only listed for a running of the factory with μ^- for simplicity. For the other polarity particles and antiparticles are exchanged. The table is taken from [33] with $misID = 20\%$.*

Detection threshold and effective volume The detection threshold is assumed to be 1 GeV [47], while for the analysis an energy window from 1 GeV to 25 GeV is introduced. The effective volume of the detector is chosen as a linear interpolation of the values given in fig. 6 in [37] in the energy variable. As a result the effective volume strongly increases with energy until it reaches about 3 Mt at an energy of 6 GeV.

Energy resolution As in [33], we chose the energy resolution function $\Delta E = \eta \cdot E$. The parameter η is varied to find out for which energy resolution the parametric resonance becomes visible. Values between $\eta = 5\%$ and $\eta = 15\%$ are looked at.

Cross section For the NC and CC cross sections of the neutrinos the predefined cross section files of GLoBES are applied. The cross sections have been determined in [48] and [49].

Systematics As a systematic error a normalization error of 2.5% for the signal and 5% for the background is assumed. This corresponds to the assumptions for the normalization error in [33].

Bin size The bin sizes are chosen to be equal within the energy range of interest. Otherwise there would be jumps in the energy spectrum due to the change of the bin size. The energy region of interest runs from 2 to 6 GeV. To guarantee that the bin size does not become larger than the energy resolution range in this energy range, the bin size is chosen as 0.1 GeV for $\eta = 5\%$, 0.2 GeV for $\eta = 10\%$, and 0.25 GeV for $\eta = 15\%$.

Oscillation parameters The oscillation parameters are taken from table 2 in [11]. For each hierarchy, the best fit values for that hierarchy have been applied.

5.3 Analysis of the event numbers

In this section the event numbers of the experiment are calculated with the GLoBES software. The parameters are selected as described in the previous section. To calculate the event numbers, GLoBES numerically folds the neutrino spectrum of the source with the oscillation probability times $\frac{1}{L^2}$, the cross section in the detector, the effective volume and the energy smearing. The resulting differential event numbers are integrated over the bin size [50].

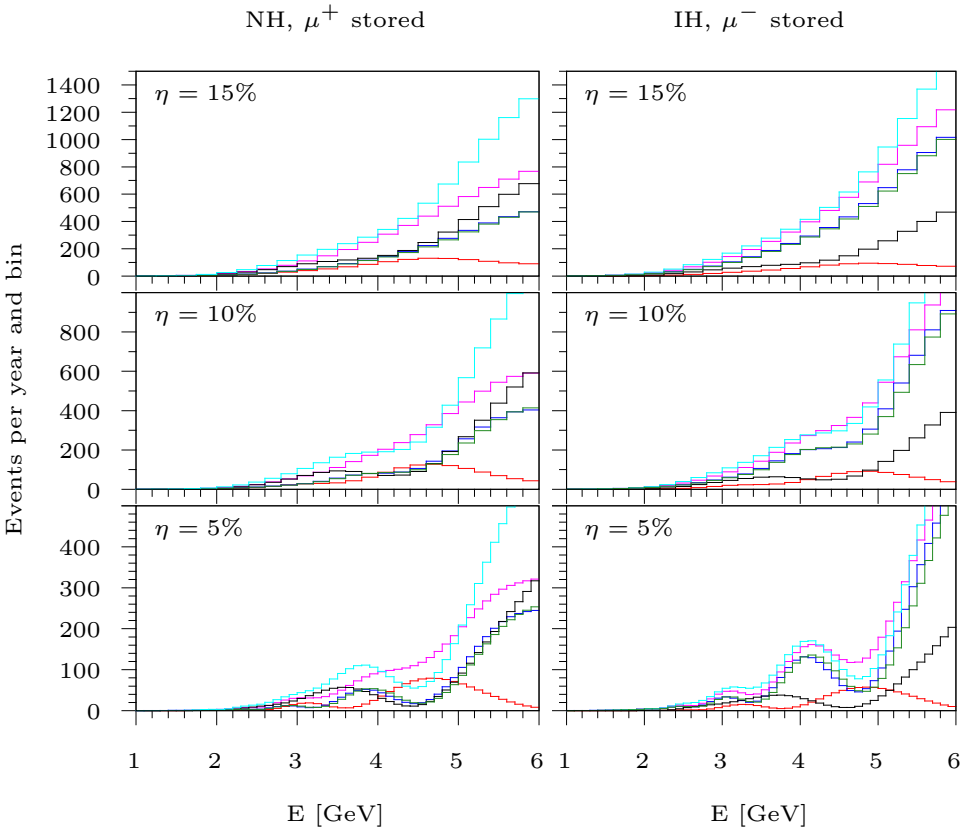

Figure 4: *Binned event numbers assuming one year of running with μ^+ and one with μ^- for selected event types. Top row: Bin width* 0.25 GeV*, energy resolution* 15%*. Middle row: Bin width* 0.2 GeV*, energy resolution* 10%*. Bottom row: Bin width* 0.1 GeV*, energy resolution* 5%*. Background events and errors are not considered. Left side (NH): Assuming averaged density: red: μ^- events, blue: μ^+ events, magenta: $\mu^- + \mu^+$ events. 3-layer density profile: black: μ^- events, green: μ^+ events, cyan: $\mu^- + \mu^+$ events. On the right side (IH), μ^- and μ^+ are interchanged.*

The results are displayed in fig. 4 for three different energy resolutions: 15%, 10% and 5%. For each energy resolution, the event numbers have been calculated for the normal hierarchy with μ^+ stored and for the inverted hierarchy with μ^- stored. These two cases have been chosen to simplify the analysis. However, a similar analysis could be done for the other two cases. The figure contains the event numbers for the single signal event types as well as the event numbers summed over both signal event types. The results for the matter pro-

files with average constant density and with three layers of constant density are displayed. The shown event numbers in this figure do not include background events and error bars. They correspond to the theoretically expected event numbers from a particular oscillation channel.

As η decreases, more details of the spectrum become visible for every event type. Considering only the μ^--events (or μ^+-events accordingly for inverted hierarchy) for the three-layer approximation (black line), we can see how the parametric resonance becomes visible: For $\eta = 15\%$, there is only a small hint of the parametric resonance, as all three resonance peaks overlap strongly. For $\eta = 10\%$, the parametric resonance peak starts to be separated from the MSW-resonance peak for the earth mantle. For $\eta = 5\%$, the MSW-resonance in the core becomes apparent as a separated peak.

Comparing the black and the red line, an increasing difference between those lines at the parametric resonance peak can be observed for decreasing η. While the parametric resonance peak becomes higher and less smeared, the oscillation minimum in the red line at this energy becomes visible. This is also observed in the total spectra for the two matter profiles (magenta and cyan). The smaller η becomes, the clearer different peaks in the spectrum become observable, and the larger is the difference between the two matter profiles around the parametric resonance.

Taking into account the μ^+-events (μ^--events for inverted hierarchy) (blue/green line), we see that the peak in the cyan line ($\mu^+ + \mu^-$ events) at the parametric resonance energy is a combination of the parametric resonance peak and a peak of the blue/green line. The peak in the blue/green line corresponds to a maximum of the muon neutrino survival probability (see fig. 2 a, blue line). The parametric resonance peak and the peak in blue/green line are not separated for any of the tested energy resolutions. Still, the parametric resonance could be studied using the charge identification method proposed in [44]. If it can reliably separate the two signal channels, the parametric resonance

might be observable for $\eta = 10\%$.

A comparison between the results for the normal and inverted hierarchy shows that the results for the inverted hierarchy are slightly worse. The event numbers for the inverted hierarchy are dominated by the muon events. A possible reason is that the cross sections for antineutrinos are slightly smaller than the ones for neutrinos. This would equalize the event numbers of the two types in the case of normal hierarchy, and lead to a domination of the μ^- events in the case of inverted hierarchy.

So far, the statistical and systematical errors of the event numbers and background events have not been taken into account. However they are relevant for the discriminability of different theoretical approaches with the studied experiment. Fig. 5 shows the sum of μ^+-, μ^--, and background-events for the three-layer density profile, the averaged density matter profile, and the assumption of no neutrino oscillations. It also includes systematical and statistical errors.

Fig. 5 shows how the errors and the background events influence the discriminability of different models: in the case of normal hierarchy, the event numbers for the three-layer approximation of the earth density profile (cyan line) are distinguishable from the event numbers without oscillations (red line) for all tested energy resolutions. The cyan line can also be discriminated from the green line representing the event numbers for the average density approximation. However, the difference is quite small. Reaching a significant difference between the event rates for the three different assumptions requires several years of data taking, and a reduction of systematical errors.

In the case of inverted hierarchy the cyan and green line can be distinguished from the red line, but not from each other for most of the energies and energy resolutions displayed. Therefore, an observation of the parametric resonance might be very difficult if the inverted hierarchy is realised in nature.

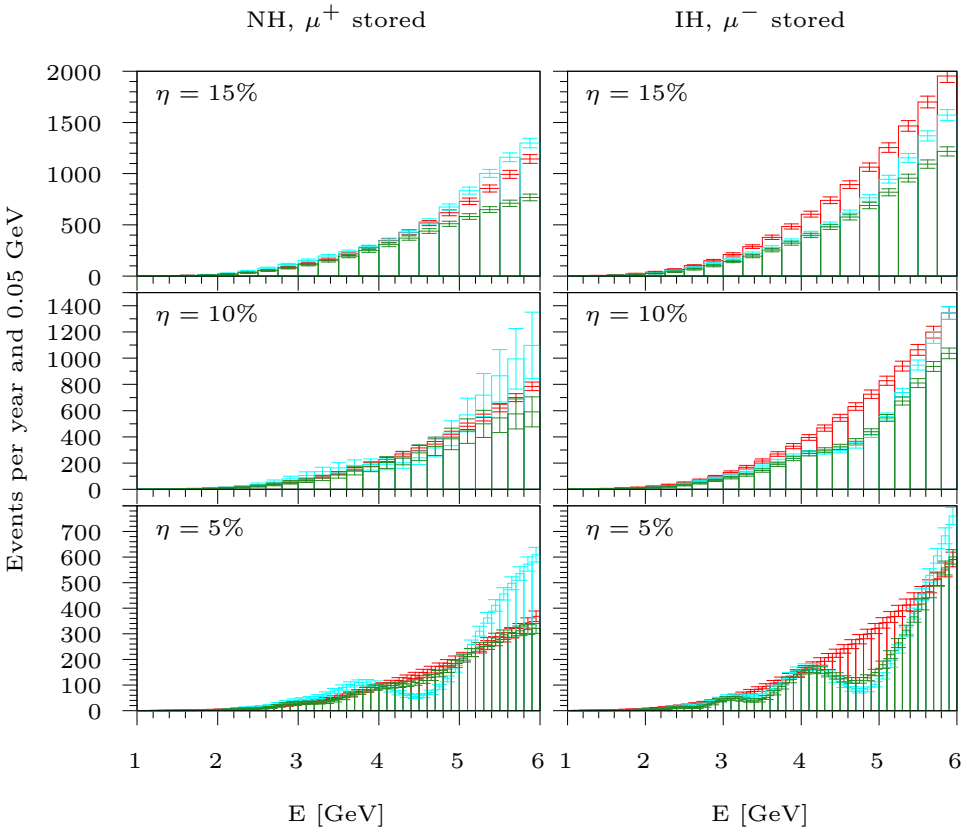

Figure 5: *Binned event numbers after one year of running with μ^+ stored (NH, left side) or μ^- stored (IH, right side) summed over all signal event types, background events included. The error bars include the systematical and statistical 1σ error. Cyan: Three-layer density profile. Green: Averaged density assumed. Red: No oscillation assumed.*

Not only the differentiation of the event numbers with the three-layer assumption from the event number without oscillations is influenced by the errors, but also the differentiation of the different peaks in the spectrum. Taking into account the systematical and statistical errors of the event numbers, a reduction of the errors might be necessary to clearly observe the parametric resonance peak at an energy resolution of 10%.

The event numbers without neutrino oscillations in fig. 5 also indicate that the increase of the event numbers towards higher energies is

not only caused by an increase of the neutrino oscillation. The figure shows clearly that the event number is only increased by oscillations in the case of normal hierarchy for the three-layer approximation, while it is suppressed by the oscillations in the other cases. The increase of the event numbers without oscillations is caused by a combination of an increasing effective volume, cross section, and flux. The strong increase of the event number around 5-6 GeV in the case of the three-layer approximation can be explained by the overlapping oscillation maxima of the two signal channels as shown in fig. 2.

To summarize: it is difficult to observe the parametric resonance with the presented setup. The parametric resonance peak can be distinguished from the mantle-MSW-peak for $\eta \leq 10\%$. The difference between the results for one layer with average density and three layers is already visible for $\eta = 15\%$, though several years of data taking might be necessary to see a significant difference. However, the μ^+ and μ^- events without background can not be differentiated by the energy resolution around the parametric resonance peak for energy resolutions of 5% or larger. They have to be separated by a different method, such as statistical separation based on the lifetime of the muons. The results for the inverted hierarchy are less significant than the results for the normal hierarchy. In this case, the parametric resonance might only be observable with an energy resolution of 5% or higher and very high statistics.

A recent report on PINGU [39] states the current energy resolution of DeepCore (the previous upgrade of IceCube) is "expected to improve by approximately 30%" [39] with the PINGU upgrade. This would lead to an energy resolution of 17.5% in PINGU. Yet, the energy resolution of PINGU would need further improvement to make the parametric resonance visible.

6 Neutrino oscillations in short two-layer baselines

On the one hand, neutrino oscillation probabilities grow with the distance travelled by the neutrino until they reach the first oscillation maximum. On the other hand, in neutrino beam experiments the flux decreases as $\frac{1}{L^2}$. In the setup described in the previous chapter, this loss of flux was compensated by a Mt-size detector. However, in many cases a compromise between the big effects achieved by a long baseline and the loss of flux has to be found.

If we want to observe matter effects, the situation is even worse. For small baselines the matter effects on the oscillation probability die out faster than the vacuum oscillations. This phenomenon is called vacuum mimicking [51]. However, the oscillation probability at short distances for a matter profile consisting of two layers has some characteristics that can help to avoid vacuum mimicking. In this chapter a setup is presented that makes use of such effects coming from a two layer matter profile rather than using a huge detector. It will be discussed how strongly a second layer can influence the results of short baseline neutrino experiments.

As in chapter 4, the oscillation probability $P_{\nu_e \to \nu_x}$ will be the tool to study neutrino oscillations in a short baseline with two layers of matter with different densities. It is tested whether such a setup could be used as an alternative to the one in the previous chapter to detect enhancement of matter effects arising from the multi-layer structure of the matter.

6.1 Short baselines and vacuum mimicking

In this section, a two-flavour approach of the neutrino oscillation probability for the short [8] baseline with a two-layer matter profile is presented. The oscillation probability is expanded in $\omega_2 L_2$. We then

[8] Throughout this chapter, short should be understood in the sense that the oscillation phase acquired after travelling this baseline is small compared to one. For large neutrino energies, such as 1-2 GeV, the length of the baseline can still be of the order of five hundred kilometres.

discuss whether the use of two layers leads to a measurable enhancement of matter effects in short baseline neutrino experiments in this approximation.

Assuming a short baseline in matter of constant density, the oscillation probability in the two-flavour approach is given by

$$P_{\nu_e \to \nu_x}(L) = \sin^2 2\theta_m \sin^2 \omega L \,. \tag{6.1}$$

If the baseline is short, $\omega L \ll 1$. This means eq. (6.1) can be expanded in this parameter. Using eq. (3.7) this expansion yields

$$P_{\nu_e \to \nu_x}(L) = s_{20}^2 \frac{\delta^2}{\omega^2} (\omega L)^2 = s_{20}^2 (L\delta)^2 \,. \tag{6.2}$$

This is the oscillation probability for a short baseline in vacuum as it can be see by expanding eq. (2.17). This simple example shows the basic idea of the vacuum mimicking effect. As the matter effects are of higher order in L than the vacuum oscillation effects, they die out faster than the vacuum oscillations when the baseline decreases.

However, this approach is only valid if the neutrino is in one of the flavour eigenstates when entering the matter. Usually, this is the case for neutrino beam experiments, but in general it is invalid for extraterrestrial sources such as the sun. If the neutrino does not enter matter in a flavour eigenstate, a more general approach using perturbation theory has to be employed [51]. Here, of particular interest is the case where the neutrino changes its flavour composition by oscillation in vacuum [9] before entering matter. In this context, the oscillation can be described by the oscillation probability for matter with two layers of different densities, as derived in section 3.3. Here $V_1 = 0$ and $V_2 = V$.

[9] Vacuum is used for the simplicity of calculation. In reality, this would not be feasible in an experiment on earth. The vacuum is then replaced by a material with small density, such as air or water.

Starting with the oscillation probability

$$\begin{aligned} P_{\nu_e \to \nu_x}(L) &= |[S]_{21}|^2 \\ &= s_{20}^2 \left(s_1^2 c_2^2 + s_2^2 c_1^2 \frac{\delta^2}{\omega^2} + 2 s_1 s_2 c_1 c_2 \frac{\delta}{\omega} + \frac{s_1^2 s_2^2}{\omega^2} V^2 \right) , \end{aligned} \tag{6.3}$$

there are two different approximations, one for a very short baseline and one for an intermediate baseline with small matter effects. In this first section, the option with the very short baseline is chosen, an expansion in $\omega_2 L_2$. The approximation for intermediate baselines will be considered in a later section.

The result of the expansion in $\omega_2 L_2$ is a simplified formula for the oscillation probability [51],

$$P_{\nu_e \to \nu_x}(L_2) \simeq s_{20}^2 \left\{ s_1^2 + (c_1^2 - s_1^2)(\delta L_2)^2 + 2 s_1 c_1 (\delta L_2) + 2 s_1^2 c_{20} (V \delta L_2^2) \right\} . \tag{6.4}$$

The very first term describes the vacuum oscillation probability in the first layer. If there is a possibility to measure the oscillation probability at the point where the neutrinos enter the second layer, this term is known, and can be ignored in the following discussion. The second and third term correspond to the increase of the oscillation probability in the second layer in the absence of matter effects. The fourth term comprises the leading order matter effects on neutrino oscillations in the second layer.

We are particularly interested in the matter effects, so the last term is the most important one. This term is proportional to $V \delta L_2^2$. However, without the first layer the leading order matter effects in neutrino oscillations as in eq. (6.4)would vanish. If the linear term is zero, the leading order term is proportional to $(V \delta L_2^2)^2$ [51]. If the phase acquired in the first layer is large enough, this means that the matter effects in the second layer can be strongly enhanced.

Due to this linear dependence on $V \delta L_2^2$, the matter effects in this setup are sensitive to the mass hierarchy of neutrinos. This fact makes

this special setup attractive not only for the measurement of matter effects, but also for the determination of the neutrino mass hierarchy.

To optimize the enhancement of the matter effects, a closer look at the approximation introduced above is necessary exploring how different ratios of the lengths of the two layers affect the matter effects on neutrino oscillations.

In a situation where the vacuum oscillations in the first layer can be ignored, there are two conditions to maximize the absolute and relative matter effects at the same time. One possibility for the relative effects to be sizeable is when the vacuum oscillation probability coming from the second layer is small. This probability is represented by the second and third term in eq. (6.4). They can be rewritten as

$$\begin{aligned}(c_1^2 - s_1^2)(L_2\delta)^2 + 2s_1c_1(L_2\delta) &= \cos(2L_1\delta)(L_2\delta)^2 + \sin(2L_1\delta)(L_2\delta) \\ &\simeq \cos(2L_1\delta)s_2^2 + \sin(2L_2\delta)s_2c_2 \\ &= s_2\left[\sin((2L_1 + L_2)\delta)\right]\end{aligned} \tag{6.5}$$

A condition for which this is equal to zero is

$$2L_1 + L_2 = n\frac{\pi}{\delta}\,, \quad n \in \mathbb{N}\,. \tag{6.6}$$

In that case, matter effects will dominate the oscillations in the second layer. To optimize the matter dependence of the oscillation even further, the fourth term in eq. (6.4) should be maximized. This can be done by setting $s_1^2 = 1$. In order to do so, $L_1\delta$ should be $\frac{\pi}{2}$. In this case, and according to the first condition, $L_2\delta$ is $n\pi$, where $n \in \mathbb{N}$. If n is zero, there will obviously be no matter effects. If δL_2 is $n\pi$, where n is any non-zero integer, $\omega_2 L_2$ is already too large for our approximation to be valid. Moreover, the baseline in this case is quite long and the benefit from a short baseline is already lost. Hence, the maximization conditions can not be fulfilled in the scope of this approach. A different approximation which allows for longer baselines is needed.

6.2 Impact of the two-layer matter density profile on intermediate baseline neutrino beam experiments

In this section, the same setup as in the previous one will be described in a different approximation. Starting again with the probability as given in eq. (6.3), the matter effects are assumed to be rather small. If the baseline is not too long, there are two small parameters, $\frac{V}{\delta}$ and VL_2. Those are still small while $\omega_2 L_2$ might already be of order one. Still, the disadvantage of this approximation is being only valid for energies below a few GeV as discussed in section 4.1, and baselines shorter than 3000 km. A Taylor expansion of eq. (6.3) in the two parameters $\frac{V}{\delta}$ and VL_2 yields

$$P_{\nu_e \to \nu_x}(L) \simeq s_{20}^2 \left\{ \sin^2(L\delta) + 2c_{20} \sin(L\delta) \left[c_{1,0} s_{2,0} \frac{V}{\delta} - \cos(L\delta) V L_2 \right] \right\} ,$$
$$L = L_1 + L_2 \,, \quad c_{i,0} = \cos(L_i \delta) \,, \quad s_{i,0} = \sin(L_i \delta) \,. \tag{6.7}$$

This approximation differs from the one in the previous chapter. The first term in eq. (6.7) is the vacuum oscillation probability in both layers. The second and third terms are the leading order matter effects on the oscillation probability coming from the second layer. This approximation has with eq. (6.4) the fact in common that the leading order matter effects are odd in δ. Therefore, the leading order matter effects are sensitive to the mass ordering. This may allow for mass hierarchy measurement if the matter effects are large enough.

Now the matter effects can be maximized, while the vacuum oscillation probability achieved in the second layer can be minimized. As the setup is not different from the one in the previous section, eq. (6.6) can be used as a first estimate for the minimization of the vacuum oscillation probability coming from the second layer. When this condition is fulfilled, eq. (6.7) reads

$$P_{\nu_e \to \nu_x}(L_1, L_2) \simeq s_{20}^2 \left\{ s_{1,0}^2 + 2c_{20} s_{1,0} c_{1,0} \left[2 s_{1,0} c_{1,0} \frac{V}{\delta} + V L_2 \right] \right\} . \tag{6.8}$$

The maximization condition for the matter effects is then given by

$$2c_{1,0}s_{1,0} = 1\,. \tag{6.9}$$

The way to fulfil this condition which leads to the shortest baseline is

$$L_1 = \frac{\pi}{4\delta} \simeq 250\,\mathrm{km}\,E(\mathrm{GeV})\,, \tag{6.10}$$

where eq. (4.11) has been used to calculate the numerical value. Together with the first condition, eq. (6.6), this determines L_2 as a function of E. The matter potential is given by V_c, as in chapter 4.1. Therefore, only the neutrino energy remains as a free parameter. Moreover, the maximization condition for the matter effects fixes $s_{1,0}$. As a result, only the matter induced part of the oscillation probability depends on E. Putting everything together, when both conditions, eq. (6.6) and eq. (6.9), are fulfilled, the oscillation probability takes the simple form

$$P_{\nu_e\to\nu_x}(E) \simeq s_{20}^2\left\{0.5 + c_{20}\left[\frac{V}{\delta} + VL_2\right]\right\} \tag{6.11}$$

$$= 0.043 + 0.019E(\mathrm{GeV})\,. \tag{6.12}$$

This result shows very clearly that the absolute matter effects, but even more the relative matter effects on the oscillation probability, can become large, albeit the matter potential is far from the MSW-resonance. It seems as if such a setup where neutrinos first oscillate in vacuum and then pass a short distance in matter could help to successfully detect matter effects enhanced by the two-layer structure of the matter profile.

Still, it is not clear that this setup will significantly increase the matter effects on neutrino oscillations compared to a usual neutrino beam experiment such as T2K [52]. In normal neutrino beam experiments neutrinos travel through matter of (approximately) constant density on the whole way from the source to the detector. The two-layer setup was meant to keep the baseline short in order to reduce the loss of flux. Anyway, only the second layer was assumed to be small in the calculations while the vacuum layer was allowed to take

every convenient length. However, flux is lost in both, the vacuum and the matter layer. To compare our setup to a normal neutrino beam experiment, the baseline of the normal experiment should be $L = L_1 + L_2$.

To be able to compare the results in a convenient way, we will consider the limiting case of the previous calculation, where $V_1 = V_2 = V_c$. The oscillation probability can be calculated from the evolution matrix as derived in section 3.3. The result is eq. (6.1). Just as before, $\frac{V}{\delta}$ and VL are assumed to be small parameters. In this case, a Taylor expansion in these parameters can be done. The result is

$$P_{\nu_e \to \nu_x}(L) = s_{20}^2 \left\{ \sin^2(L\delta) + 2c_{20} \sin(L\delta) \left[\sin(L\delta)\frac{V}{\delta} - \cos(L\delta)VL \right] \right\} , \quad L = L_1 + L_2 \, . \tag{6.13}$$

This formula looks very similar to eq. (6.7). The vacuum induced part of the oscillation probability is exactly the same in both formulas. As expected, there are two small differences in the terms describing the matter effects on neutrino oscillations.

The first difference is that the term proportional to $\frac{V}{\delta}$ does not contain $c_{1,0}s_{2,0}$ as in eq. (6.7), but rather $\sin(L\delta) = c_{1,0}s_{2,0} + c_{2,0}s_{1,0}$. As long as $L_i\delta < \frac{\pi}{2}$, $i = 1, 2$, $\sin(L\delta) > c_{1,0}s_{2,0}$. In that case, the first term describing the matter effects is smaller in the case with two layers. If δL_i becomes bigger than $\frac{\pi}{2}$, the baseline is already quite large. Focusing on short to medium length baselines, this will not be discussed. Anyway, at this length scale a two-layer matter density profile might be difficult to realise.

The second difference between eq. (6.7) and eq. (6.13) is that the last term on the right side of eq. (6.7) is proportional to VL_2 while the last term on the right side of eq. (6.13) is proportional to $V\,L$ for one layer. It is obvious, that $V\,L$ is bigger than VL_2. Still, this term enters with a minus sign thus lowering the matter induced part of the oscillation probability. In other words, contrary to the term proportional to

$\frac{V}{\delta}$ this term yields a lower matter induced oscillation probability for a normal neutrino beam experiment. As a consequence, it is not obvious whether an increase of matter effects can be achieved by letting the neutrino travel the first part of its way from the source to the detector through vacuum.

Just as in eq. (6.7), the leading order matter effects in eq. (6.13) are odd in δ. As a consequence, the question in which setup the impact of the mass hierarchy is larger is the same as the question in which setup the leading order matter effects are larger. This question can be answered by numerical estimates.

As the vacuum oscillation probability is the same for both setups, it will be ignored. Solely, the focus is on the matter induced part of the oscillation probability,

$$P^{mat}_{\nu_e\to\nu_x,\,2}(L) = 2s^2_{20}c_{20}\sin(L\delta)\left[c_1 s_2 \frac{V}{\delta} - \cos(L\delta)VL_2\right] \tag{6.14}$$

for the setup with two layers and

$$P^{mat}_{\nu_e\to\nu_x,\,1}(L) = 2s^2_{20}c_{20}\sin(L\delta)\left[\sin(L\delta)\frac{V}{\delta} - \cos(L\delta)VL\right] \tag{6.15}$$

for the setup with only one layer.

Fig. (6) shows $P^{mat}_{\nu_e\to\nu_x,\,2} - P^{mat}_{\nu_e\to\nu_x,\,1}$ for different energies as a function of L_1 and L_2. It happens that the biggest deviation from zero takes place for low energies. For energies of 2 and 3 GeV (bottom row), the difference of the two probabilities is nearly zero. For lower energies (top row), the result is negative for most combinations of L_1 and L_2. Only for $E = 0.5\,\mathrm{GeV}$, and $L \simeq 600\,\mathrm{km}$ the results become positive. For such a long baseline the setup with two layers, especially such a long baseline in vacuum, is difficult to realize. But if such a setup can be realized, it might help to observe an enhancement of matter effects on neutrino oscillations due to a two-layer structure of the matter profile. It might also help to determine the mass hierarchy.

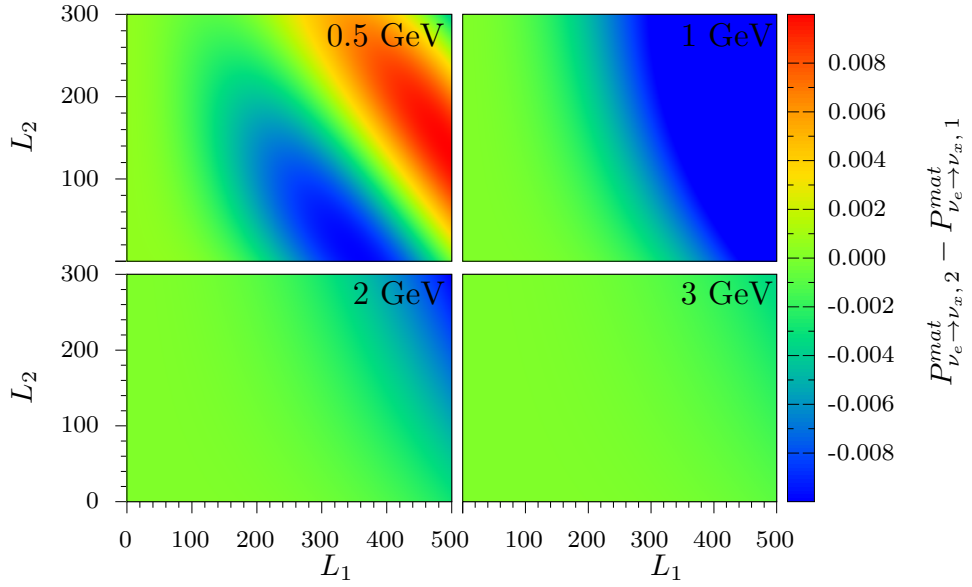

Figure 6: *Difference of the matter induced parts of the oscillation probability for one and two layers, $P^{mat}_{\nu_e\to\nu_x,2} - P^{mat}_{\nu_e\to\nu_x,1}$, as given by eq. (6.14) and eq. (6.15), for neutrino energies of 0.5, 1, 2 and 3 GeV as a function of the length of the two layers, L_1 and L_2*

To put it briefly, in most cases the additional effort for a two-layer setup does not bring any advantage. Only in the special case where $E = 0.5\,\text{Gev}$ and $L \simeq 600\,\text{km}$, the oscillation probability induced by matter is bigger for the two-layer setup. However, in this case the vacuum part of the baseline is rather long. Moreover, this estimate has not taken into account the energy spectrum of the neutrino which could wash out the effect. Thus, using two layers does not help to shorten the overall baseline, but only the part of the baseline in matter. An enhancement of the oscillation by the two-layer structure will be very difficult to achieve. Hence, the benefits of the two-layer structure might not compensate for the additional effort to build it.

6.3 The short baseline with two layers using the example of atmospheric neutrinos

The setup discussed above is realized by one important neutrino source: atmospheric neutrinos. The author of [51] discusses the enhancement

of matter effects on the neutrino oscillation probability by the oscillation in the atmosphere before entering the earth. He utilizes the approximation given in eq. (6.4). His study will be extended by using the approximation derived in the previous section. Furthermore it will be discussed whether the energy- and angular resolution of current detectors are good enough to resolve the enhancement of the matter induced part of the oscillation probability.

In our atmosphere, cosmic particles scatter with the atoms of the atmosphere. In this process mesons, mostly pions, are produced. Neutrinos emerge from their decay and the decay of the muons originating from this decay. The flux of these neutrinos is a mixture of neutrinos and antineutrinos. It contains electron and muon neutrinos [53,54]. On average, the production process takes place at a height of $h = 15\,\mathrm{km}$ above the ground. Depending on the nadir angle θ_n [10] the neutrinos coming to a detector travel the distance

$$L_1 = -R\cos\theta_n + \sqrt{(R+h)^2 - R^2\sin^2\theta_n} \tag{6.16}$$

through the atmosphere [11], where $R = 6371\,\mathrm{km}$ is the radius of the earth. After that, neutrinos traverse the earth and reach the detector after a distance of

$$L_2 = 2R\cos\theta_n\,. \tag{6.17}$$

Neutrinos with an energy of 0.5-3 GeV travelling nearly horizontally are considered so the nadir angle is in the range of 82-90°. For those neutrinos the approximation given by eq. (6.7) can be used.

This section is dedicated to the question whether it is important to take into account the oscillations in the atmosphere of the earth in the analysis of the data on nearly horizontally entering neutrinos from atmospheric neutrino experiments. In addition, it will be addressed whether current atmospheric neutrino experiments might observe an

[10] The nadir angle is assumed to be smaller than $\frac{\pi}{2}$. Otherwise the neutrinos do not travel through the earth.

[11] The density of the atmosphere is small compared to the density of the earth. For that reason the atmosphere can be considered as vacuum. This simplifies the calculations.

enhancement of the matter effects on neutrino oscillations due to the oscillation in the atmosphere. To answer this, some numerical estimations are done.

The oscillation probability and the matter induced part of the oscillation probability are computed as given in eq. (6.7) and eq. (6.13) as functions of E and θ_n. For the effective matter potential, V_c is used.

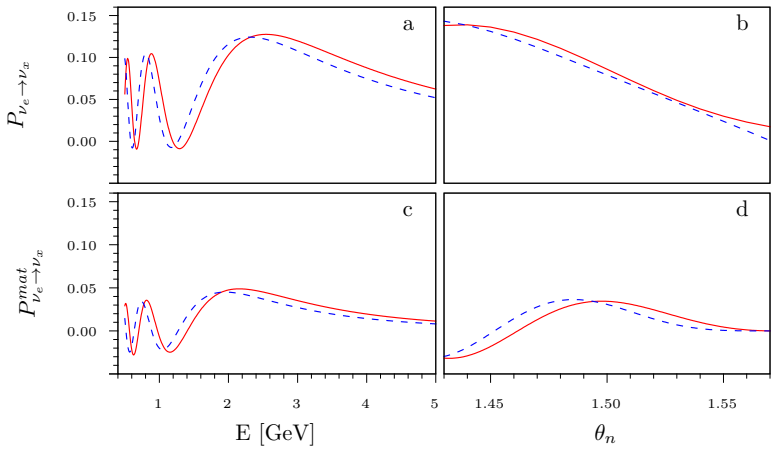

Figure 7: *Upper row: Total oscillation probability* $P_{\nu_e \to \nu_x} = P_{\nu_e \to \nu_\mu} + P_{\nu_e \to \nu_\tau}$ *taking into account oscillations in the atmosphere (red solid line, see eq. (6.7)) and assuming neutrino production at the surface of the earth (blue dashed line, see eq. (6.13). Bottom row: The same for the oscillation probability with the total oscillation probability in vacuum subtracted,* $P^{mat}_{\nu_e \to \nu_x}$ *(see eq. (6.14) for red solid and eq. (6.15) for blue dashed line). Left column: Function in dependence of* E *for* $\theta_n = 1.47$*. Right column: Function in dependence of* θ_n *for* $E = 1.5\,\mathrm{GeV}$*.*

Fig. 7 shows the calculated quantities. The red solid lines represent the oscillation probabilities with the oscillations in the atmosphere. The blue dashed lines stand for the calculation where oscillations outside of the earth have been neglected completely and the production point of the neutrinos is assumed to be at the surface of the earth. The plots on the left side show the energy dependence. It is visible that the probability is strongly oscillating for small energies. For higher energies above 2.5 GeV, the probability slowly decreases. At these energies, the probability that takes the oscillations in air into account is

slightly bigger. Another difference between the red and the blue line: compared to the blue line, the oscillation maxima and minima of the red line are always reached for slightly higher energies than the ones for the blue line. As a result, at certain energies the oscillation probability concerning oscillations in air becomes larger than the probability neglecting them while for other energies it is the other way round.

The right graphs exhibits the same probabilities as a function of the nadir angle. Here, the energy is fixed. The oscillation of the probability with varying θ_n is less fast than the one with varying E. In graph d we monitor that similar to the observations in graph a and c, the red line reaches its maximum for higher θ_n and then decreases slower than the blue line. However, one does not observe a strong enhancement of the oscillation probability by the additional layer in air.

Overall, it seems that the oscillation in the atmosphere can have a big influence on the oscillation probability, but this effect strongly depends on the energy. Nevertheless, in experiments, the energy and the angle can not be measured with a very high accuracy yet. For example, the energy resolution of the Super-Kamiokande experiment is about 17-30% for multi-GeV events [55]. In order to get more realistic results the oscillation probability is now averaged over the uncertainty range of the angle and the energy.

Fig. 8 shows the integrated oscillation probability. Here, an energy resolution of $0.17E$ has been assumed. This corresponds to the best resolution for multi-GeV events in the Super-Kamiokande detector [55]. The angular resolution of θ_n is 0.26 [55]. As this error range covers the complete span of angles considered, the plot does not show the integrated probabilities as a function of θ_n. Instead, the integration over θ_n is always done from 1.2 to 1.57.

Compared to the results before integration, we see that the oscillations have been washed out. The dependencies of the oscillation probability and its matter-induced part on the neutrino energy have de-

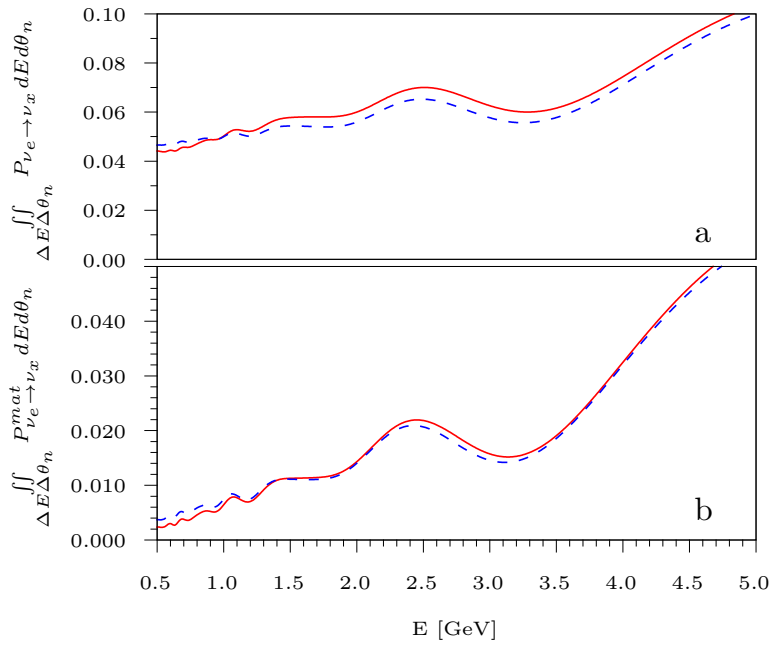

Figure 8: *a: Total oscillation probability $P_{\nu_e \to \nu_x}$ taking into account oscillations in the atmosphere (red solid line) and assuming zero production height (blue dashed line) integrated over the nadir angle from 1.2 to 1.57 and over the neutrino energy interval $[E - \delta E, E + \delta E]$, as a function of the mean neutrino energy E. $\delta E = 0.17E$. b: The same graph for the oscillation probability with the total vacuum oscillation probability subtracted, $P^{mat}_{\nu_e \to \nu_x}$.*

creased. Furthermore, the difference between the red and the blue line is now rather small for all energies. Especially the difference between the matter effects on neutrino oscillations for the two assumptions has become tiny. The big differences we saw in fig. (7) have averaged out.

In conclusion: as long as the energy and angle resolution of future atmospheric neutrino experiments do not become better by some orders of magnitude, the oscillation in the atmosphere can be neglected, as the effect is completely washed out by averaging over the large E- and θ_n-resolution ranges. No enhancement of the oscillation probability caused by the two-layer setup is observed.

7 Conclusions

This thesis has dealt with three different setups for neutrino beam experiments that include matter with multiple layers of constant density. In the first part a setup with alternating layers of different constant densities has been studied. The objective has been to test whether it would be possible to build such a matter density profile in order to observe parametric enhancement of neutrino oscillations. To do so, the required baseline for an observation under idealized conditions has been computed. It turned out that the baseline has a lower bound which is independent of the neutrino energy. If the matter profile consists of alternating layers of lead and vacuum, this bound is about 1200 km, for vacuum and the crust of the earth it is even 3900 km. Hence, such an artificial density profile can not be built in such a way that it serves the observation of the parametric enhancement of neutrino oscillations.

The second part of this thesis has examined the question of sending a neutrino beam through the core of the earth. In particular, an experiment in which a neutrino beam is send from a neutrino factory at RAL, the most northern neutrino facility, to PINGU at the south pole has been simulated with the GLoBES software. The event numbers have been plotted for different energy resolutions of the detector testing which energy resolution is needed to observe the parametric resonance of neutrino oscillations in the earth. The event numbers for a three-layer approximation of the earth density profile have been compared to the event numbers obtained with a constant density approximation of the earth density profile and without neutrino oscillations. The result of this comparison has been that the event numbers obtained with the two different density approximations already differ for an energy resolution of 15%. However, the parametric resonance peak becomes visible in the spectrum at an energy resolution of between 15% and 10%. The two signal channels can not be separated around the parametric resonance by energy resolution for energy resolutions of 5% or larger. A careful analysis using statistical charge discrimination would have to be employed. Moreover several years of runtime increasing the

statistics might be necessary to observe a significant deviation between the predicted event numbers of the different theoretical assumptions. In addition, these observations require an improvement of the currently expected energy resolution of the PINGU upgrade.

The last part of the thesis has dealt with neutrino oscillations in short baselines. The possibility has been discussed to enhance the matter effects on neutrinos passing a short distance in matter by letting them pass a certain distance in vacuum before or after the distance in matter. Under certain conditions, which are similar to the parametric resonance condition, this allows for an enhancement of the matter effects. It has been questioned whether this could help to increase the matter effects in short baseline neutrino experiments. It has turned out that one would need a long baseline in vacuum (at least 300 km) to benefit from the two-layer setup compared to the situation when the whole distance is travelled in matter. It has been addressed if the effects described in this section might be important in the prediction for atmospheric neutrino experiments. But any enhancing effect coming from oscillations in the atmosphere averages out as soon as the realistic energy and angular resolutions of the detector are taken into account.

As a conclusion, it has proven very difficult to observe the parametric resonance or similar enhancement effects arising from multiple layers of matter with different densities. None of the setups discussed in this thesis is well-suited to detect such a resonance. Artificial profiles fulfilling all necessary conditions are hard to build. In contrast, the earth in general allows for parametric resonance, but it is difficult to reach the required energy resolution to disentangle different resonances. The effects arising in short baselines with a two-layer structure are small and suffer from finite energy resolutions.

Nonetheless, an improvement of the energy resolution of current detectors and long-time observations might lead to the observation of the parametric resonance of neutrinos passing through the core of the earth.

References

[1] Y. Fukuda *et al.*, "Evidence for oscillation of atmospheric neutrinos," *Phys. Rev. Lett.*, vol. 81, pp. 1562–1567, 1998, hep-ex/9807003.

[2] Y. Abe *et al.*, "Indication for the disappearance of reactor electron antineutrinos in the Double Chooz experiment," *Phys. Rev. Lett.*, vol. 108, p. 131801, 2012, 1112.6353.

[3] J. K. Ahn *et al.*, "Observation of Reactor Electron Antineutrino Disappearance in the RENO Experiment," *Phys. Rev. Lett.*, vol. 108, p. 191802, 2012, 1204.0626.

[4] F. P. An *et al.*, "Observation of electron-antineutrino disappearance at Daya Bay," *Phys. Rev. Lett.*, vol. 108, p. 171803, 2012, 1203.1669.

[5] M. Apollonio *et al.*, "Search for neutrino oscillations on a long baseline at the CHOOZ nuclear power station," *Eur. Phys. J.*, vol. C27, pp. 331–374, 2003, hep-ex/0301017.

[6] L. Wolfenstein, "Neutrino Oscillations in Matter," *Phys. Rev.*, vol. D17, pp. 2369–2374, 1978.

[7] S. P. Mikheev and A. Yu. Smirnov, "Resonance Amplification of Oscillations in Matter and Spectroscopy of Solar Neutrinos," *Sov. J. Nucl. Phys.*, vol. 42, pp. 913–917, 1985. [Yad. Fiz.42,1441(1985)].

[8] E. K. Akhmedov, "Neutrino oscillations in inhomogeneous matter. (In Russian)," *Sov. J. Nucl. Phys.*, vol. 47, pp. 301–302, 1988. [Yad. Fiz.47,475(1988)].

[9] V. K. Ermilova, V. A. Tsarev, and V. A. Chechin, "Parametric enhancement of neutrino oscillations in matter. (In Russian)." [Short Notice of the Lebedev Institute], 1986.

[10] P. I. Krastev and A. Yu. Smirnov, "Parametric Effects in Neutrino Oscillations," *Phys. Lett.*, vol. B226, pp. 341–346, 1989.

[11] M. C. Gonzalez-Garcia, M. Maltoni, and T. Schwetz, "Global Analyses of Neutrino Oscillation Experiments," *Nucl. Phys.*, vol. B908, pp. 199–217, 2016, 1512.06856.

[12] B. Pontecorvo, "Mesonium and anti-mesonium," *Sov. Phys. JETP*, vol. 6, p. 429, 1957. [Zh. Eksp. Teor. Fiz.33,549(1957)].

[13] B. Pontecorvo, "Inverse beta processes and nonconservation of lepton charge," *Sov. Phys. JETP*, vol. 7, pp. 172–173, 1958. [Zh. Eksp. Teor. Fiz.34,247(1957)].

[14] Z. Maki, M. Nakagawa, and S. Sakata, "Remarks on the unified model of elementary particles," *Prog. Theor. Phys.*, vol. 28, pp. 870–880, 1962.

[15] B. Kayser, "Neutrino physics," *eConf*, vol. C040802, p. L004, 2004, hep-ph/0506165.

[16] G. Altarelli and K. Winter, eds., *Neutrino Mass*. Springer Verlag, 2003. chapter 1 and 5.

[17] F. W. Bullock and R. C. E. Devenish, "LEPTON SPECTROSCOPY," *Rept. Prog. Phys.*, vol. 46, p. 1029, 1983.

[18] E. K. Akhmedov and A. Yu. Smirnov, "Paradoxes of neutrino oscillations," *Phys. Atom. Nucl.*, vol. 72, pp. 1363–1381, 2009, 0905.1903.

[19] C. Giunti and C. W. Kim, "Coherence of neutrino oscillations in the wave packet approach," *Phys. Rev.*, vol. D58, p. 017301, 1998, hep-ph/9711363.

[20] N. Schmitz, *Neutrinophysik*. Teubner Studienbücher, 1997.

[21] M. Kobayashi and T. Maskawa, "CP Violation in the Renormalizable Theory of Weak Interaction," *Prog. Theor. Phys.*, vol. 49, pp. 652–657, 1973.

[22] E. K. Akhmedov, R. Johansson, M. Lindner, T. Ohlsson, and T. Schwetz, "Series expansions for three flavor neutrino oscilla-

tion probabilities in matter," *JHEP*, vol. 04, p. 078, 2004, hep-ph/0402175.

[23] W. C. Haxton and B. R. Holstein, "Neutrino physics," *Am. J. Phys.*, vol. 68, pp. 15–32, 2000, hep-ph/9905257.

[24] E. K. Akhmedov, "Parametric resonance of neutrino oscillations and passage of solar and atmospheric neutrinos through the earth," *Nucl. Phys.*, vol. B538, pp. 25–51, 1999, hep-ph/9805272.

[25] E. K. Akhmedov, P. Huber, M. Lindner, and T. Ohlsson, "T violation in neutrino oscillations in matter," *Nucl. Phys.*, vol. B608, pp. 394–422, 2001, hep-ph/0105029.

[26] T.-K. Kuo and J. T. Pantaleone, "Neutrino Oscillations in Matter," *Rev. Mod. Phys.*, vol. 61, p. 937, 1989.

[27] H. A. Bethe, "A Possible Explanation of the Solar Neutrino Puzzle," *Phys. Rev. Lett.*, vol. 56, p. 1305, 1986.

[28] W. C. Haxton, "The solar neutrino problem," *Ann. Rev. Astron. Astrophys.*, vol. 33, pp. 459–503, 1995, hep-ph/9503430.

[29] E. K. Akhmedov, M. Maltoni, and A. Yu. Smirnov, "1-3 leptonic mixing and the neutrino oscillograms of the Earth," *JHEP*, vol. 05, p. 077, 2007, hep-ph/0612285.

[30] A. de Gouvea, A. Friedland, and H. Murayama, "The Dark side of the solar neutrino parameter space," *Phys. Lett.*, vol. B490, pp. 125–130, 2000, hep-ph/0002064.

[31] P. J. Mohr and D. Newell, "Physical Constants." `http://pdg.lbl.gov/2015/reviews/rpp2015-rev-phys-constants.pdf`, 2015. last visit on 26.07.16.

[32] H. Binder, *Lexikon der chemischen Elemente*. S. Hirzel Verlag, 1999.

[33] J. Tang and W. Winter, "Requirements for a New Detector at the South Pole Receiving an Accelerator Neutrino Beam," *JHEP*, vol. 02, p. 028, 2012, 1110.5908.

[34] W. Winter, "Neutrino mass hierarchy determination with IceCube-PINGU," *Phys. Rev.*, vol. D88, no. 1, p. 013013, 2013, 1305.5539.

[35] K. Dick, M. Freund, P. Huber, and M. Lindner, "Masses and mixings from neutrino beams pointing to neutrino telescopes," *Nucl. Phys.*, vol. B588, pp. 101–109, 2000, hep-ph/0006090.

[36] D. R. Williams, "Earth fact sheet." `http://nssdc.gsfc.nasa.gov/planetary/factsheet/earthfact.html`, 5 2016. last visit on 26.07.16.

[37] M. G. Aartsen *et al.*, "Letter of Intent: The Precision IceCube Next Generation Upgrade (PINGU)," 2014, 1401.2046.

[38] S. K. Agarwalla, T. Li, O. Mena, and S. Palomares-Ruiz, "Exploring the Earth matter effect with atmospheric neutrinos in ice," 2012, 1212.2238.

[39] J. P. Yañez, "From DeepCore to PINGU: Measuring atmospheric neutrino oscillations at the South Pole," *EPJ Web Conf.*, vol. 116, p. 11009, 2016, 1601.05245.

[40] P. Huber, M. Lindner, and W. Winter, "Simulation of long-baseline neutrino oscillation experiments with GLoBES (General Long Baseline Experiment Simulator)," *Comput. Phys. Commun.*, vol. 167, p. 195, 2005, hep-ph/0407333.

[41] P. Huber, J. Kopp, M. Lindner, M. Rolinec, and W. Winter, "New features in the simulation of neutrino oscillation experiments with GLoBES 3.0: General Long Baseline Experiment Simulator," *Comput. Phys. Commun.*, vol. 177, pp. 432–438, 2007, hep-ph/0701187.

[42] A. M. Dziewonski and D. L. Anderson, "Preliminary reference earth model," *Phys. Earth Planet. Interiors*, vol. 25, pp. 297–356, 1981.

[43] S. Choubey *et al.*, "International Design Study for the Neutrino Factory, Interim Design Report," 2011, 1112.2853.

[44] C. Saji, *Study of upward-going muons in Super-Kamiokande*. PhD thesis, Niigata University, 2002. chapter 10.

[45] M. Freund, P. Huber, and M. Lindner, "Extracting matter effects, masses and mixings at a neutrino factory," *Nucl. Phys.*, vol. B585, pp. 105–123, 2000, hep-ph/0004085.

[46] M. A. Markov and I. M. Zheleznykh, "Large Scale Cherenkov Detectors in Ocean, Atmosphere and Ice," *Nucl. Instrum. Meth.*, vol. A248, pp. 242–251, 1986.

[47] S. Wren, "Neutrino Mass Ordering Studies with PINGU and IceCube/DeepCore," 2016, 1604.08807.

[48] E. A. Paschos and J. Y. Yu, "Neutrino interactions in oscillation experiments," *Phys. Rev.*, vol. D65, p. 033002, 2002, hep-ph/0107261.

[49] M. D. Messier, *Evidence for neutrino mass from observations of atmospheric neutrinos with Super-Kamiokande*. PhD thesis, Boston U., 1999.

[50] P. Huber, J. Kopp, M. Lindner, M. Rolinec, and W. Winter, "GLoBES User's and experiment definition manual." `https://www.mpi-hd.mpg.de/personalhomes/globes/documentation/globes-manual-3.1.8.pdf`, 10 2010. last visit on 26.07.16.

[51] E. K. Akhmedov, "Matter effects in oscillations of neutrinos traveling short distances in matter," *Phys. Lett.*, vol. B503, pp. 133–139, 2001, hep-ph/0011136.

[52] H. M. O'Keeffe, "Current status and near future plans for T2K," 2016, 1605.00821.

[53] S. Choubey, "Atmospheric Neutrinos: Status and Prospects," 2016, 1603.06841.

[54] G. Gelmini and E. Roulet, "Neutrino masses," *Rept. Prog. Phys.*, vol. 58, pp. 1207–1266, 1995, hep-ph/9412278.

[55] M. Ishitsuka, *L/E analysis of the atmospheric neutrino data from Super-Kamiokande*. PhD thesis, Tokyo U., 2004.

Erklärung

Ich versichere, dass ich diese Arbeit selbstständig verfasst und keine anderen als die angegebenen Quellen und Hilfsmittel benutzt habe.

Heidelberg, den ...,